DEVELOPMENT AND TESTING OF SPRAY-COATED LIGHTNING STRIKE PROTECTION SYSTEMS FOR FIBER-REINFORCED THERMOPLASTIC COMPOSITES

A Thesis by

Clay Parten

Bachelor of Science, University of Houston, 2016

Submitted to the Department of Mechanical Engineering
and the faculty of the Graduate School of
Wichita State University
in partial fulfillment of
the requirements for the degree of
Master of Science

December 2019

DEVELOPMENT AND TESTING OF SPRAY-COATED LIGHTNING STRIKE PROTECTION SYSTEMS FOR FIBER-REINFORCED THERMOPLASTIC COMPOSITES

The following faculty members have examined the final copy of this thesis for form and content, and recommend that it be accepted in partial fulfillment of the requirement for the degree of Master of Science, with a major in Mechanical Engineering.

Ramazan Asmatulu, Committee Chair

Davood Askari, Committee Member

Krishna Krishnan, Committee Member

DEDICATION

To my mother, who has always been there for me

ACKNOWLEDGMENTS

I would like to thank the many individuals whose help was instrumental in the completion of my thesis work. First, I owe a debt of gratitude to everyone at the National Institute for Aviation Research Environmental Test Lab (NIAR ETL) who supported me every step of the way. Thanks to Michelle Cronkleton and Alyssa Gonzales for believing in me and sparking the decision to choose this thesis subject. Thanks to Rebeka Khajehpour for ongoing discussions about everything science and research and all her help with writing of this thesis. I can't thank Brock Milford enough for trying to explain electrical theory to me, and donating his time and expertise on the DEL Generator. Thanks to Billy Martin, Jeff Phillips and Kyle McMullen for their support, and for allowing me permission to use the facilities at the NIAR (ETL). Thanks also to everyone at the NIAR Advanced Coatings Lab. Brandon Hunt not only allowed me access to his facilities; he was also patient with me as a beginner in the spray-coatings realm. Both Brandon, and Manish Shinde were instrumental in support of this thesis and have contributed paint, equipment, supplies, knowledge, time and a great deal of guidance. So much gratitude goes to Justina Calbert, the Advanced Spray Coatings lab technician who did the actual spray-coating and most of the documentation and characterization work. Without her, I would not have finished this thesis on time. Thanks to Gregory Martin for allowing me to use his NIAR Research Lab microscope for sample characterization. I would also like to thank Davood Askari, the professor central to advancing my knowledge of composites and supportive advisor along the way. I also owe a debt of gratitude to Ramanan Sritharan for helping me grapple with the experimental process, as well as the thesis process. Lastly, I extend my gratitude to Ramazan Asmatulu for all his efforts as my primary advisor, and for helping guide me through my

graduate experience. I also thank Triumph Aerospace Structures for donating seven composite panels for this project.

ABSTRACT

This project investigated a conductive nanomaterial spray-coated lightning strike protection (LSP) for thermoplastic composites (TPCs) for use on aircraft exterior surfaces. The aerospace industry has expressed increasing interest in TPCs for future aircraft due to processing and material advantages over thermoset composites (TSCs). TPC components can be joined by induction welding, allowing a significant weight savings in comparison to joining by fasteners. However, current metallic LSP systems interfere with the induction welding process. A post-processed, economically viable, spray-coated LSP would solve the induction welding interference problem. In Phase One of this study, four nano and sub-micro conductive LSP coatings were formulated and tested for surface conductivity. The two best candidates were further developed and prepared for spray-coating tests. Phase Two entailed spray-coating six TPC panels with selected LSP and performing Zone 2A lightning strike testing. Two variations of silver coated copper (Ag/Cu) were selected as the conductive filler with 15% and 30% silver content, respectively. Two loading levels of 55 wt% and 70 wt% were tested in an epoxy carrier. Challenges in spray-coating with the 70 wt% loading caused the resistance to be higher than 55 wt% panels. Despite the lower conductive coating weight and higher resistance, the 70 wt% panels performed better than 55 wt% panels. The higher silver content Ag/Cu30 also produced marginally better LSP results. With further development, spray-coated Ag/Cu sub-micro flakes could be a viable, economical post-processed LSP system.

TABLE OF CONTENTS

TABLE OF CONTENTS (continued)

Chapter Page

LIST OF TABLES

LIST OF FIGURES

LIST OF FIGURES (continued)

LIST OF FIGURES (continued)

LIST OF ABBREVIATIONS / NOMENCLATURE

Ag/Cu20	Silver Coated Copper Flake – 20% Silver
Ag/Cu30	Silver Coated Copper Flake – 30% Silver
AGATE	Advanced General Aviation Transport Experiment
ARP	Aerospace Recommended Practice
BMI	Bismaleimide
CM1	Conductive Material 1
CM2	Conductive Material 2
CNFP	Carbon Nanofiber Paper
CNT	Carbon Nanotube
CFRP	Carbon Fiber Reinforced Polymer
CuNW	Copper Nanowire
DEL	Direct Effects of Lightning
ECF	Expanded Copper Foil Lightning Strike Protection
ETL	Environmental Test Laboratory
FAA	Federal Aviation Administration
GNP	Graphene Nano Platelets
HBN	Hexagonal Boron Nitride
IPA	Isopropyl Alcohol
ITO	Indium Tin Oxide
KART	Kansas Aviation Research and Technology Growth Initiative
LM PAEK	Low Melt Polyaryletherketone
LSP	Lightning Strike Protection

MWCNT	Multi-Walled Carbon Nanotube
NIAR	National Institute of Aviation Research
NP	Nanoparticle
OEM	Original Equipment Manufacturer
PBLS	Phosphor Bronze Lightning Strike Protection
PEEK	Polyetheretherkeytone
PET	Polyethylene Terephthalate
PETG	Glycol-Modified Polyethylene Terephthalate
PPS	Polyphenylenesulfide
PVP	Polyvinlypyrrolidone
SAE	Society of Automotive Engineers, Aerospace
SWCNT	Single Walled Carbon Nanotube
TPC	Thermoplastic Composite (Carbon Fiber)
TSC	Thermoset Composite (Carbon Fiber)
Uni	Unitape Carbon Fiber Composite
Wt%	Weight Percent

CHAPTER 1

INTRODUCTION

1.1 Motivation

In recent years, the use of advanced composite materials in the aerospace industry has begun to replace metal due to the ongoing quest for weight reduction. In addition, the high specific strength and stiffness as well as corrosion resistance compared to aluminum and other metals makes composites a favorable choice [1], [2]. The constituents of these structural composites have been carbon fiber in a thermoset, predominantly epoxy, matrix.

Composites do, however, have a disadvantage when subjected to lightning strike. Unlike aircraft with a metal surface structure, composite aircraft components lack the conductivity to quickly conduct the charge away from the lightning strike attachment point. When the energy dwells in a small area a great deal of heat is generated, leading to violent damage to the structure. For this reason, composites are in need of surface protection which increases their conductivity, thereby reducing the likelihood of damage to the structure.

The industry is now beginning a turn towards thermoplastic matrix composites (TPCs) because of their advantages, such as increased chemical resistance, faster processing times, and higher fracture toughness, compared to thermoset composites (TSCs) [3], [4]. In addition, TPC components can be welded without the need for an additional adhesive through techniques like induction welding, ultrasonic welding, or friction welding [5]. This bonding technique creates a homogenous bond between the two sections, equivalent to the bond between lamina. This process leads to a great reduction in the thousands of fasteners that are used over an entire commercial aircraft, and thus a great weight savings. Like TSCs, TPCs need added surface protection from lightning strikes due to their lack of conductivity relative to metal. The dataset

for lightning strike damage and protection of epoxy-based composites is significant and still growing. However, thus far, there is little data on the effects of lightning and the methods of protecting thermoplastic composite structures.

1.2 Problem Statement

On average, commercial aircraft are struck by lightning between 1000 and 10,000 flight hours. This translates to approximately one lightning strike per year [6]. The current in a severe lightning strike event can be as high as 200 kA. Multiple mechanisms of a lightning strike cause damage to an aircraft. The primary causes of lightning strike damage are acoustic shock effects, resistive temperature rise, melting or burning at attachment points and magnetic (Lorentz) force effects. Other problems may arise as a consequence of the primary mechanisms such as arcing or sparking at bonds or, if the damage is enough to penetrate through the laminate, ignition of vapors in fuel tanks or damage to internal electrical systems. These issues could potentially lead to catastrophic failure or loss of control of the aircraft [2], [6]–[9].

Aircraft with metal exterior surfaces are well suited to handling lightning strikes due to the high conductivity of the material which rapidly dissipates the current across the surface and thereby lessening the concentration of energy in one area while protecting the passengers and electronics on the interior, as well as fuel tanks that are integrated into the wings. Composite materials have low conductivity compared to metals and, without additional surface protection, are not conductive enough to prevent severe damage to the affected area. For this reason, both thermoplastic and thermoset resin based composites require additional conductive material added to the surface layer in order to increase the dissipation of energy of a lightning strike over a large area, thus reducing the damage [2], [6], [10], [11]. The current solution for protection of exterior

composite structures is to co-cure a metallic mesh or interwoven wire on the surface layer which increases the conductivity of the outer layer to levels approaching a metal component.

Commercial aircraft manufacturers are exploring induction welding as a method of bonding thermoplastic composite components together, greatly reducing the need for metal fasteners. This is one advantage of TPCs over TSCs, since TSCs cannot be induction welded. Thousands of fasteners are employed on commercial aircraft and their elimination would mean a significant weight savings. This new manufacturing method will benefit from a form of lightning strike protection (LSP) which can be applied after the components are induction welded, since a pre-consolidated metallic LSP would act as a Faraday cage, disrupting the magnetic field and thereby making induction welding impossible. Development and testing of a spray-coated conductive nanomaterial based LSP that can be applied after welding of TPC aircraft components is the subject of this research.

1.3 Research Objectives

Phase One of this research focused on investigating processing methods of four LSP nanomaterials: graphene nanoplatelets/carbon nanotubes (GNPs/CNTs), two variations of copper coated silver sub-micro flakes (Ag/Cu20, Ag/Cu30), and copper nanowires (CuNWs). The goal here was to optimize the electrical conductivity of the surface layer, while maintaining the surface durability of the epoxy matrix with the least possible weight penalty.

In Phase Two of this research, the most successful candidates from Phase One were integrated into a spray-coating system for application to carbon fiber/low-melt Polyaryletherketone (LM PAEK) thermoplastic composite test panels. Two panels included a spray-coated dielectric thermal protection layer using hexagonal boron nitride (HBN) micro particles below the

conductive layer. The panels were tested for resistance to lightning strike damage according to the following test standards: SAE ARP 5412B, SAE ARP 5414A, and SAE ARP 5416A.

CHAPTER 2

LITERATURE REVIEW

2.1 The Lightning Environment

2.1.1 Environmental Lightning

Lightning is generated as a result of charge development primarily within cumulonimbus clouds. The three types of lightning are referred to as intra-cloud, inter-cloud and cloud-to-ground, respectively, and are illustrated in Figure 1. [12], [13].

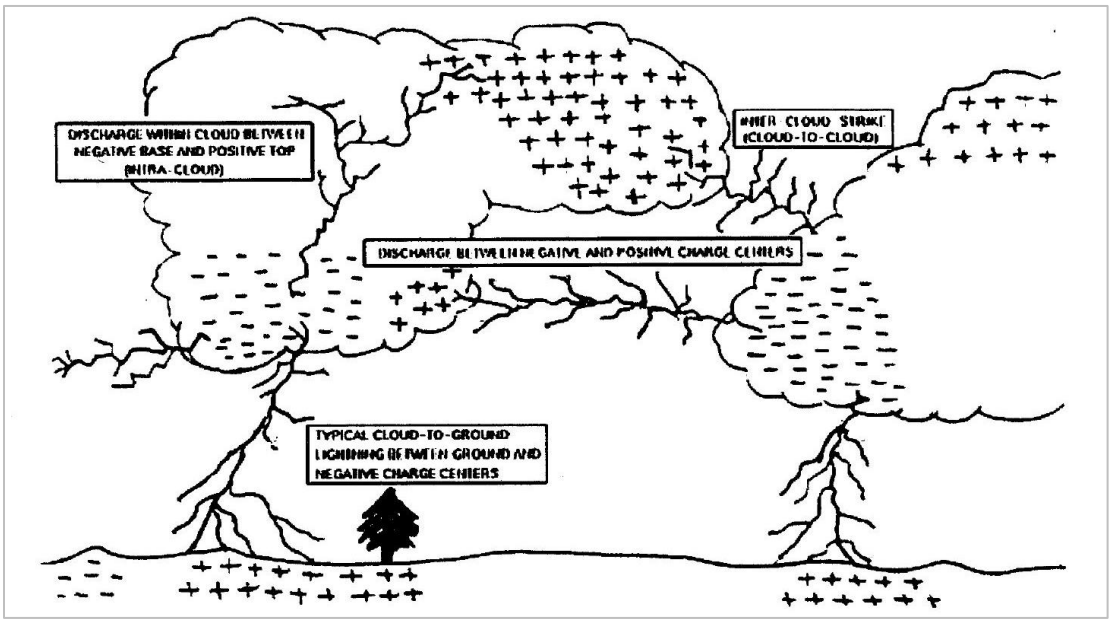

Figure 1. Illustration of cloud region charge polarity depicting three general types of lightning: inter-cloud, intra-cloud and cloud-to-ground [13].

Leading up to a lightning strike, the upper regions of the cloud become predominantly positively charged and the lower regions predominantly negatively charged due to the rising and falling motion of freezing and liquid droplets within the cloud. A discharge occurs when the electric potential between the cloud and surrounding environment exceeds the breakdown strength of the air, thus resulting in ionization. This breakdown results in an ionized column known as a leader, which occurs at about 30kV/cm at sea level conditions. Lightning may occur

between regions within a cloud, regions of opposing polarity in nearby clouds or between clouds and the ground.

In the case of cloud-to-ground lightning, if the lower region of a polarized cloud tends to be negatively charged, then the surface directly beneath the cloud will become positively charged as electrons on the surface are repelled and forced into the ground. When the electric field is sufficient, junction leaders will extend upward from high points extending from the earth's surface such as trees, mountain tops or tall buildings. The stepped leader following the path of greatest voltage potential gradient will meet one of the upward projecting junction leaders at a switching point to complete the channel and close the circuit. This event allows all free electrons in the ionized channel to move to neutralize the charge resulting in current pulse amplitudes as high as 200 kA with extremely rapid rise times to peak. This current pulse results in extreme frictional heating energy and thus rapid expansion of the surrounding air. This event is known as the first return stroke.

2.1.2 Lightning Interaction with Aircraft

The advent of a lightning strike begins with a stepped leader propagating out from a charge center in a cloud in the direction of the highest local gradient in the electric field surrounding the source. Since an aircraft is essentially a conductor assuming the electric potential of its location, the extremities of an aircraft also divert and compress equipotential field lines as illustrated in Figure 2 [7]. The compression of field lines represents a steeper voltage gradient and therefore the most probable pathway for propagation of a leader.

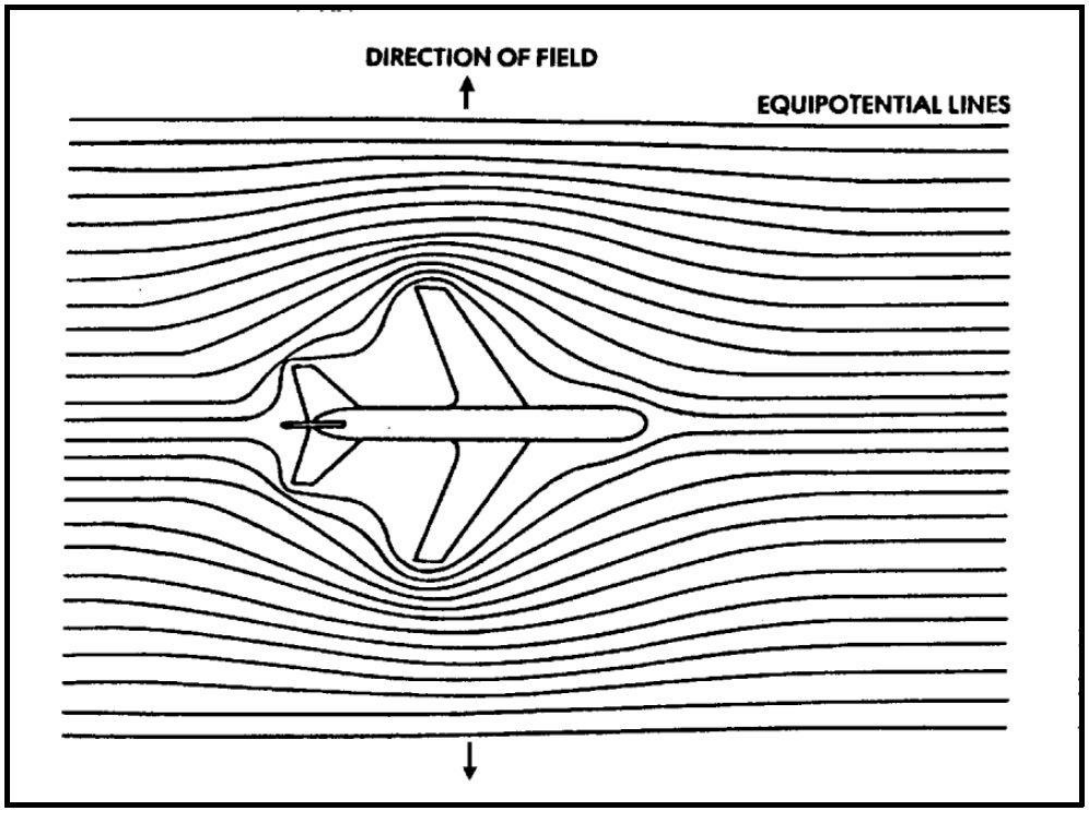

Figure 2. Compression of equipotential lines around extremities of an aircraft [7].

Numerous airborne studies conducted from the 1960s to the 1980s [14] have provided ample evidence that aircraft are often the origination point of a lightning strike. Leaders can propagate out from the extremities of the aircraft towards oppositely charged regions [6], [13]. Research programs conducted by the ONERA/CEV Transall test program [14] and others [7] have shown that lightning strikes commonly originate from the aircraft when flying through a region that has an intense electric field. In either case, if the leader from the aircraft and the cloud are in close enough proximity to meet one another, the aircraft conducts the current to its final destination of opposite charge. This event is captured in Figure 3.

Figure 3. In flight commercial aircraft struck by lightning with conduction path over the metal surface from cloud, to aircraft, to ground [15].

Once the flash channel circuit is complete, a high current return stroke occurs, as previously described. This return stroke can have a rise time of less than 100μs and a peak amplitude in excess of 200kA in extreme cases. Currents can continue to flow through the channel for durations of up to and exceeding one second [14].

2.1.3 Aircraft Lightning Strike Zones

SAE ARP 5414A standard defines lightning strike zones on aircraft according to expected lightning current levels. Initial attachment and exit points on an aircraft where the electric field intensity is high include the nose, wingtips and other extremities. These areas, defined as Zone 1 regions have the highest probability of initial attachment and first return strokes. Zone 2 regions, which include the fuselage, are susceptible to swept strokes. Swept strokes occur due to the forward motion of the aircraft over the duration of the lightning strike. [7], [8]. Zone 3 regions must conduct lightning current between points of attachment. More specific zone definitions, as illustrated in Figure 4, are the following: **Zone 1A**— Aircraft

surfaces where the probability of the first return stroke is high during attachment of the lightning channel, with low probability of flash hang-on. **Zone 1B**— Aircraft surfaces for which a first return stroke is of lower amplitude and is likely to occur during attachment of the lightning channel, with low probability of flash hang-on. **Zone 1C**— Aircraft surfaces for which the first return stroke with low amplitude is expected, and there is low probability of flash hang-on. **Zone 2A**— Aircraft surfaces along which swept return strokes are expected with a low probability of flash hang-on. **Zone 2B**— Aircraft surfaces along which swept return strokes are expected with a high probability of flash hang-on. **Zone 3**— Aircraft surfaces other than Zones 1A, 2A, 1B or 2B for which there is a low probability of lightning channel attachment lying in between other zones. These areas conduct significant current between other zones[7].

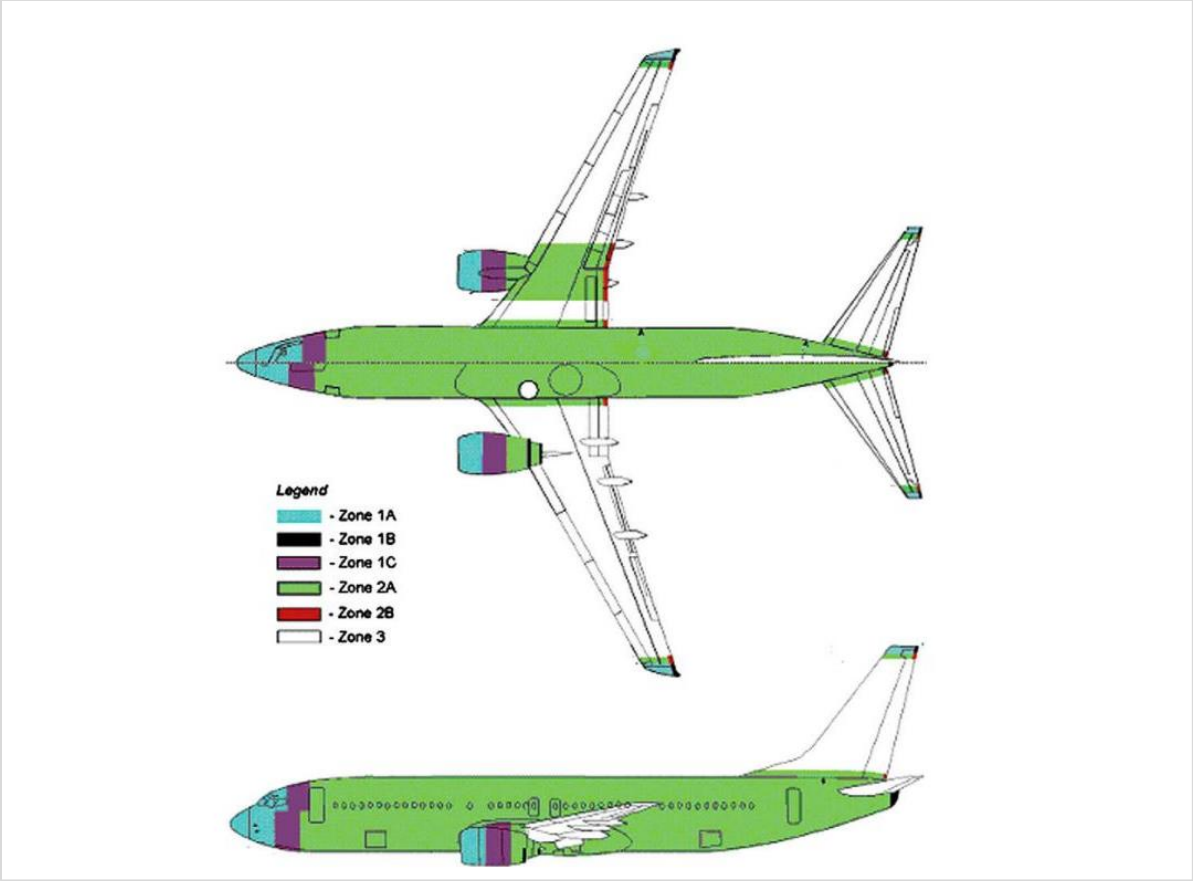

Figure 4. Lightning strike zones defined by SAE ARP 5414 [7].

2.1.4 Simulated Lightning Components

In 1972, the Society of Automotive Engineers (SAE) formed a subcommittee to improve lightning strike test standards at the request of the Federal Aviation Administration (FAA) and US Department of Defense. As a result a committee was formed to develop and standardize lightning protection requirements for aircraft, designated SAE AE-4L. The committee's first report established a severe lightning strike waveform as well as standardized testing methods. The waveform consisted of current components A, B, C and D (which are designed to represent a spectrum of the most commonly encountered forms of lightning) [12].

Figure 5 shows the four current components along with their electrical characteristics and common effects on aircraft structures.

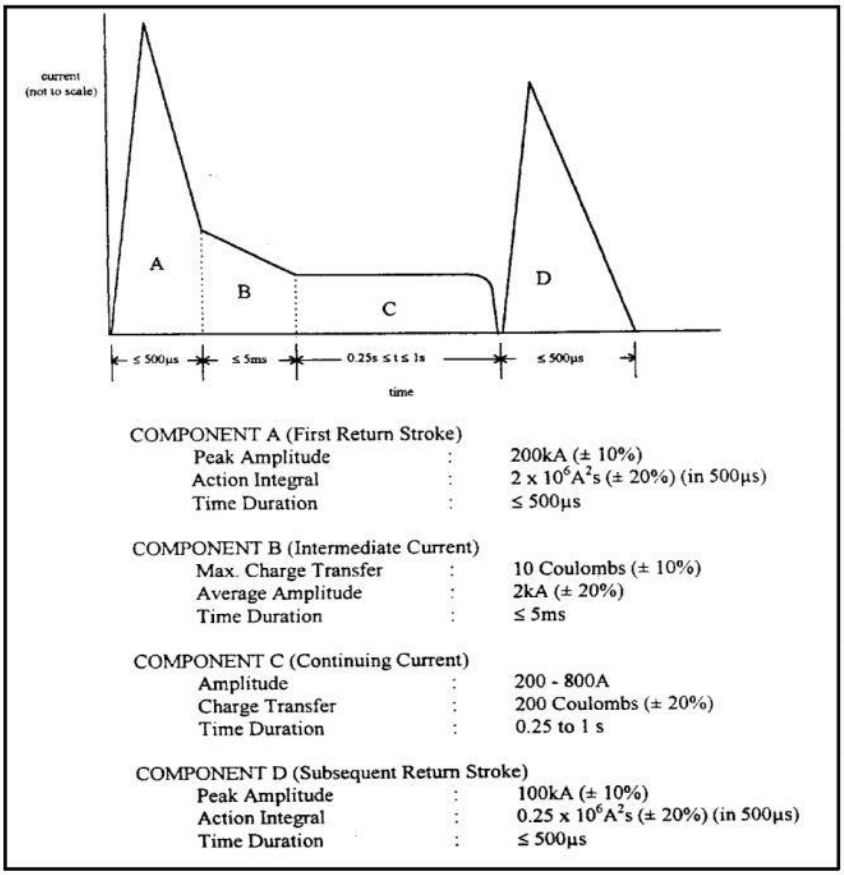

Figure 5. Standardized aircraft lightning environment [12].

Current component A mimics the effects of the first return stroke in a cloud-to-ground stroke and represents the high current strike associated with cloud-to-ground lightning first return strokes. Component A carries shockwave effects due to rapid heating of the surrounding air and magnetic force effects due to rapid change of current. Component D represents one subsequent return stroke and is most responsible for depositing the Zone 2A energy. Intermediate and continuing currents are represented by both B and C components.

The Action Integral is defined in Lightning Protection of Aircraft as "the ability of the current to deposit energy in a resistive object." (A^2*s or Joules/Ohm), as well as "joules of damaging energy deposited per ohm of resistance of an article into which the current is injected." This parameter is used to quantify the level of power contained in a component A or D. Both components B and C represent intermediate current and continuing current [12].

2.2 Composite Aircraft Materials

2.2.1 Overview

A composite is the combination of at least two macroscopic materials in order to form a new material whose properties are an improvement over the constituents [16]. Adobe, the combination of sun dried mud and straw used as a building material for thousands of years is an early example of a composite material [17]. Concrete is another composite material made from cement and rocks and more recently strengthened with re-bars [16]. Fiberglass is among the most common modern composite materials. It was first utilized on a large scale in boat building during World War II due to its advantageous strength-to-weight ratio and ease of manufacturing [18]. Advanced composites for aerospace applications are highly engineered materials optimized for use in aircraft, as well as the challenges of space flight. Boeing's 787 Dreamliner and Airbus's

A350XWB both extensively utilize composite materials to save weight while preserving strength and stiffness of structures [19].

2.2.2 Fiber Materials

Contemporary aircraft commonly employ carbon fibers produced from a polyacrylonitrile (PAN) precursor. The PAN is first chemically treated and spun into fibers under tension. Then the fibers are stabilized against fusion during final high temperature processing in a process known as stabilization, between 700°C and 1500°C. Then the graphitization process uses an inert gas atmosphere with temperatures between 1200°C and 3000°C to improve the crystalline structure of the carbon fiber. A final step, called sizing, is a chemical surface treatment to protect fibers during processing and increase wettability with the intended matrix. Depending on processing parameters and precursor materials, the strength and modulus of the fibers can be modified to suit the application, and can be as high as 5000 Mpa and 400 Gpa, respectively, or even higher [20], [21].

2.2.3 TSC and TPC Matrix Material

Structural aircraft composite components have, until very recently, predominantly employed epoxy resin-based thermosets as the matrix material due to its high compressive strength, good environmental stability, and ability to transfer loads between fibers while maintaining the shape and stiffness of the structure. Thermoplastic matrix composites have some desirable properties that make them an enticing alternative to epoxy matrix composites: melt processing rather than chemical processing, higher fracture toughness, and fewer consumables, like vacuum bagging materials, needed. Some drawbacks are higher temperature and pressure required, and the lack of drapability, since the thermoplastic matrix is a solid at room temperature [16], [22].

The processing of TSCs involves a chemical reaction between the base polymer and a curing agent, which can occur at room temperature once the two components are thoroughly mixed. In the case of most advanced composite structures, the composite is prepared as a pre-impregnated unit, or "prepreg", where the fibers are impregnated with the mixed resin and stored until use below zero degrees Celsius in a partially cured state, requiring a curing cycle at elevated temperatures in the range of 150°C to 180°C to complete the chemical reaction. Even in cold storage, aerospace-grade thermoset composites have a limited shelf life before they expire. In aerospace structural applications, the fabrication of parts almost always includes autoclave processing to achieve elevated pressures in order to eliminate voids and compress plies for optimal fiber-to-matrix volume ratio. However, an autoclave is not required for curing the resin. Thermoset polymer chains form a cross-linked structure while curing. The degree of cross-linking is dependent on cure temperature and cooling rate [20]. Once cured, the structure can no longer be altered.

The polymer used in TPCs, on the other hand, requires a different set of processing procedures. Thermoplastics do not cure by a chemical reaction like an epoxy thermoset. Thermoplastics such as polyetheretherketone (PEEK), polyphenylenesulfide (PPS), and "low melt" polyaryletherketone (LM PAEK) are processed by heating above their melting temperatures, from 260°C to 360°C, depending on the polymer, where they become viscous fluids. As the polymer cools, it re-solidifies. Aerospace grade TPCs are partially crystalline and the percent crystallinity is dependent on the chemical makeup as well as the cooling rate. Thermoplastics require alternate processing methods since, even above the melting temperature, their viscosity is orders of magnitude higher than that of thermoset resins, which makes it difficult to process TPCs using the same processes used for TSCs. In addition, since the melting

temperature of these engineering thermoplastics is between 270°C and 360°C, the most common part fabrication techniques to date are matched-die molding, where the composite is pressed between A and B side heated metal molds at high pressure in order to consolidate the part. Autoclave/vacuum bag processing and tape laying, among other techniques, are also available for TPC structures depending on the application. [23], [24]

A recent study by Kamiyama et al. compared the lightning strike damage of un-protected carbon fiber composites with three different matrix resins: epoxy, bismaleimide (BMI), and polyetheretherketone (PEEK). The first two are thermoset resins. Epoxy is the standard in the aerospace industry for ambient temperature applications with the onset of thermal decomposition around 280°C. BMI is a high temperature resistant thermoset resin with thermal decomposition onset at 370°C. PEEK is a thermoplastic resin also with good high temperature performance and thermal decomposition beginning at about 530°C. The results indicated a relationship between higher thermal breakdown temperature and less lightning strike damage. In addition, the higher fracture toughness of PEEK resin was cited as the reason for comparatively less delamination of the carbon fiber/PEEK composite samples [4]. This result suggests the possibility that the increased fracture toughness and higher temperature tolerance of select thermoplastic resins may reduce the extent of LSP necessary to protect susceptible aircraft exterior components from lightning strike damage.

2.2.4 Lightning Strike Protection Materials

The most common practice for LSP of thermoset matrix composites has been to include a conductive metallic mesh or a layer of hybrid carbon and metallic wire fabric in the surface layer of the laminate during layup in order to increase the surface conductivity of the composite. Extensive lightning strike testing has been performed confirming reduced damage with certain

types of LSP [2], [7] . To date, no carbon nanomaterial-based LSP is used by major OEMs on commercial aircraft.

The five main types of contemporary lightning strike protection for composite materials are listed here [2]:

- Solid Metal Foils: Solid foils are desirable for their high conductivity, but impractical in application due to the difficulty of layup over curved surfaces and the tendency for delamination [2]. They are also heavy, which is due to their continuous coverage, negating weight savings provided by the composite structure.
- Metal Coated Fibers: Metal-coated fibers are used to increase the electrical conductivity of a dedicated top layer of a composite layup. These composites are fabricated either by chemical vapor deposition or electrocoating processes [2]. Metal-coated fibers that have been used include aluminized fiberglass. Drawbacks to this material include increased damage compared with other forms of LSP when tested with surface finish and aluminum, which corrodes in contact with carbon fiber, and has been virtually eliminated as a material choice for LSP in aerospace applications [7]
- Woven Metal Mesh and Hybrid Mesh: Metal meshes are machine woven and as a result of the over-under weave pattern have a double thickness, and therefore higher resistivity, at the intersections. In one review article [2], the authors referenced an article on the Composites World website [25], claiming that woven mesh has been used on the Boeing 787. This article actually only briefly describes the LSP as interwoven wire, far more likely referring to a layer of woven carbon fabric with metallic wire interwoven along each fiber during fabrication.

- Expanded Metal Foils: Solid foils have excellent conductivity but suffered application problems such as wrinkling over curved surfaces and poor adhesion. The solid layer of metal also adds considerable weight to the structure and was eventually abandoned as a form of LSP. Expanded metal meshes begin with a solid foil, which is then perforated and expanded to form a mesh. The mesh is then pressed flat for a uniform layer thickness. This is currently the most common form of LSP in service on commercial composite aircraft because of its conformability and high conductivity [2].
- Conductive Metallic Particle Films and Sprays: A conductive metal spray-coated LSP system that utilizes a silver particle conductive filler is available for commercial use. The spray version is only intended for use on Zone 2A components, while the film version is intended for either Zone 2A or Zone 1A components. The high silver content makes this product very expensive.

2.3 LSP of Composites

2.3.1 Nanomaterials

Thin film coatings for LSP made of highly conductive nanofibers, including carbon nanotubes, graphene nanoplatelets and metallic nanowires have been investigated as an alternative to metal meshes. There are many ways of fabricating a conductive nanocoating including electroplating, cold spray, vacuum bagged mold processing, and spray coating, among others. Several methods will be reviewed in the proceeding section. Their light weight and good conductivity satisfies some primary considerations for application of LSP. Research in this area thus far has not achieved the same level of protection as copper mesh owing to lower conductivity of the discontinuous nanofiller. [4], [11], [26]–[31]

A study by Han et al. [26] combined buckypaper with an additional adhesive layer between the carbon nanotube (buckypaper) layer and the composite. Researchers tested panels with a conductive adhesive, pure epoxy film and one with boron nitride. It was found that more lightning strike damage occurred to the buckypaper-protected composite panels with a conductive adhesive (~1.0 wt% CNTs) than with an insulating adhesive containing HBN at approximately 20 wt%, and with the neat epoxy falling in between in performance. This was partly attributed to a conduction path through the thickness of the conductive adhesive to the composite layer, and also to the increased thermal energy tolerance of the boron nitride loaded insulating layer. Figure 6 shows a micrograph cross section of the laminate and LSP with a 200 µm thick HBN insulating layer.

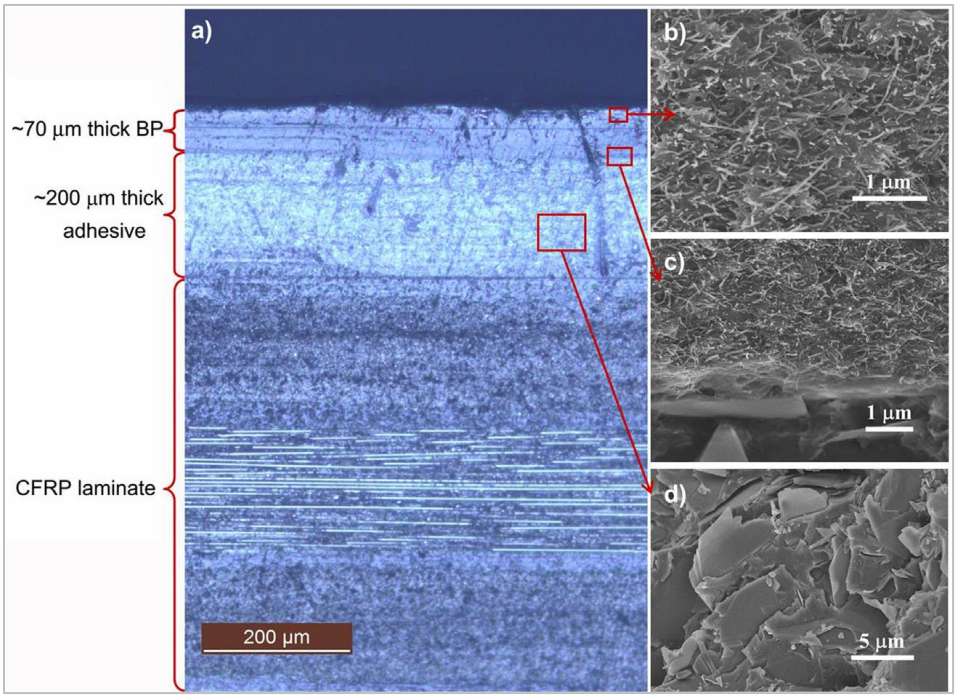

Figure 6. Cross-section image of laminate and LSP with 200 µm thick HBN insulating layer (a) optical microscope image of the cross section, (b, c and d) SEM images of red rectangular area shown in (a) [26].

A form of nanofiber LSP studied by Gou et al. [28] combined carbon nanofibers with nickel nanostrands fabricated by the papermaking process. In this study, a temporary nanoclay

layer was sprayed onto the uppermost layer of carbon nanofiber paper (CNFP) before infusion with resin in order to prevent the resin from seeping through the porous surface. This method resulted in a maximum surface conductivity of 340 S/cm after consolidation with the composite via resin infusion which compressed and flattened the CNFP. Three variations were prepared. The first, a single layer with an equal wt% of carbon nanofibers and nickel nanostrands with a latex binder (CNFP-1); the second; two layers–one consisting of only carbon-nanofiber and the second a mix of both materials, with a latex binder (CNFP-2); third, two layers with the same wt% mix, but produced as one homogeneous layer without binder (CNFP-3). SEM images of these three variations at 1um resolution are shown in Figure 7.

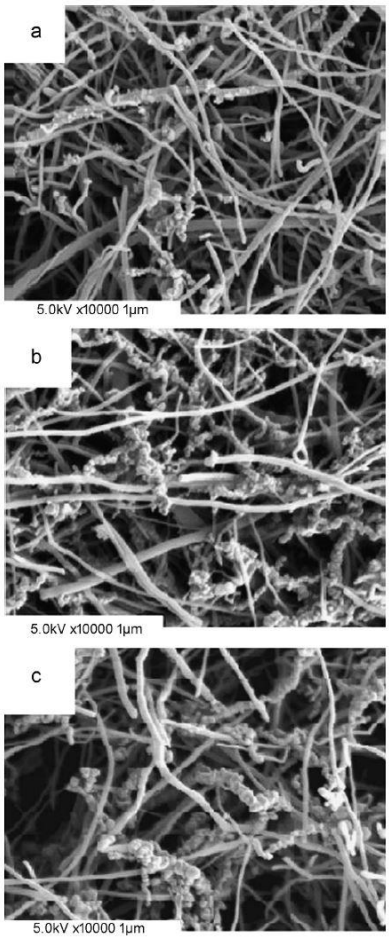

Figure 7. SEM images of top surface of carbon nanofiber paper:
(a) CNFP-1, (b) CNFP-2, (c) CNFP-3 [28].

The most damage occurred on the CNFP-1 sample, which had the least energy-absorbing mass and the lowest conductivity. CNFP-3 sustained the least damage when subjected to a 2A lightning strike because of the combination of the increased energy absorption capability through added mass, increased thermal tolerance by the highest loading of nickel nanostrands and the greatest electrical conductivity.

The percolation threshold is the wt% loading of a discontinuous conductive material in a non-conductive matrix at which the composite transitions from being an electrical insulator to becoming a conductor. With respect to nanomaterials in a polymer matrix, there are many factors which influence the threshold value, including the type of polymer, processing method of the composite, synthesis method of the nanomaterial, and whether the nanomaterial has been functionalized. A great deal of research has been conducted on CNTs and graphene in numerous polymer matrices with widely varied percolation thresholds from 0.005 wt% to as high as 7 wt% [32]–[34]. Most research is in agreement that conductivity is reduced when CNTs are functionalized in comparison to their non-functionalized equivalent [32], [33], [35], [36]. Likewise, the percolation threshold in terms of wt% is a small transition range, which sees a conductivity increase by six or more orders of magnitude, but plateaus near the percolation level even up to much higher loading levels [33].

Thermal conductivity may also play a role in protecting the composite substrate from damage if resistive heating can be quickly dissipated. A study in 2005 by Moisala et al. [32] studied thermal conductivity as well as electrical percolation threshold loading (0.005 – 0.5 wt%) of multi-walled carbon nanotubes (MWCNTs) and single-walled carbon nanotubes (SWCNTs) in an epoxy matrix. The thermal conductivity for MWCNTs proved to be far greater than that for SWCNTs at each loading level. In addition, the thermal conductivity of SWCNTs

initially decreased with increased loading, remaining below the conductivity of pure epoxy at all loading levels, while the thermal conductivity of MWCNTs increased up to 0.29 W/mK.at 0.5 wt%. In the same study electrical conductivity of the MWCNTs also exceeded that of SWCNTs by at least an order of magnitude up to the maximum loading. Some discrepancies could be attributed to differences in production methods of nanotubes. The MWCNTs were grown by chemical vapor deposition and not functionalized, while the state of the purchased SWNTs necessitated pre-dispersion. These were either chemically dispersed or separated by ball-milling. Previous work by [37] suggests that the electrical conductivity of MWCNTs may be carried by the outermost shell possibly due to the interlayer resistivity and isolation and possibly other factors such as alternate layer structure, thereby creating a switching between metallic and semi-conducting layers. Regardless of the mechanism, this paper suggests the number of shells has little contribution to electrical conductivity.

2.3.2 Nanomaterial Dispersion

There are several physical routes to good dispersion, including mechanical stirring, shear mixing, centrifugal mixing, ball milling and three roll milling. These methods are often combined to optimize results depending on the viscosity of the resin system, size and type of filler nanomaterial, level of loading, and other factors. Chemical functionalization has also been used for dispersion purposes with great success and long term stability.

Chemical functionalization also often makes use of harsh acids that can alter or damage the crystalline structure of the nanofiller, thereby reducing its conductivity [33]. In other cases, surfactants are used which helps separate the individual nanofillers and makes dispersion easier, but the surfactant coating is difficult to remove, again reducing conductivity [34]. Overall results are mixed for their effectiveness in increasing electrical conductivity [33], [35], [36].

2.3.3 Nanomaterials for LSP

The method of protecting TPCs from lightning strike damage is nearly identical to that of protecting TSCs. Because of its higher processing temperatures and higher viscosity, LSP with a thermoplastic polymer as the carrier for the conductive nanofiller requires alternative processing techniques to integrate the sub-micro or nanofillers into thin polymer films. The methods of processing TPCs include melt impregnation, powder impregnation, the commingling of matrix and reinforcement fibers, and solvent impregnation [5], [23], [38]. Since thermoplastics are solid at room temperature, solvent processing would seem to be the most likely alternative for spray-coating. However, given the excellent chemical resistance of engineering thermoplastics such as LM PAEK, only the harshest of solvents can be used at elevated temperatures. On the other hand, an epoxy-based resin system will bond to a thermoplastic composite with proper substrate preparation [38], [39]. For these reasons, the scope of this research is limited to an epoxy-based carrier for the conductive nanofiller.

Li et al. [41] explored the effects of spray-coated hybrid CNTs/GNPs for enhanced electrical and thermal surface conductivity of CFRP laminates. CNTs and GNPs were suspended in acetone for spray-coating on carbon fiber/epoxy composite panels. The resulting coating was then spray-coated with an epoxy top layer. Electrical resistivity was measured through the depth by sanding layers down and measuring at successive exposed layer depths. The result is depicted graphically in Figure 8. Optimal surface resistivity was about 1 ohm/sq, with decreasing resistivity as depth increased, with a minimum resistivity of 3e-4 ohm/sq at a depth of 180 microns.

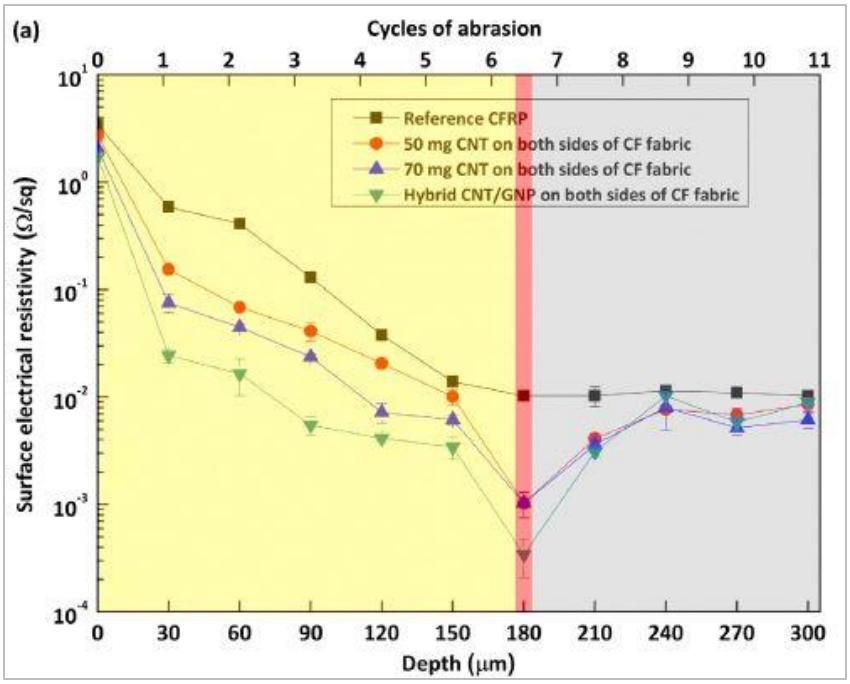

Figure 8. Surface resistivity with respect to sanding depth into conductive coating [41].

Zhang et al. [11] researched the galvanic corrosion of metallic meshes and alternative nanocomposite spray-coatings on CFRPs. Their research showed that copper and aluminum corroded in a naturally occurring galvanic cell coupled with carbon fiber in various electrolytic solutions. In the same study, graphene and indium tin oxide (ITO) nanomaterials were separately added into epoxy primer carriers and sonicated for dispersion before spray coating onto carbon fiber panels to a thickness of 3 mils. Nanomaterial loading levels were incrementally increased for each material. The maximum loading of graphene was 8wt% due to limits associated with agglomeration, while the maximum loading of ITO was 40 wt% with no agglomeration issues. Resulting electrical conductivities for graphene and ITO coatings at maximum loading were 52.22 S/m (1.92 ohms/cm) and 1366 S/m (0.07 ohms/cm), respectively.

Metallic nanomaterials have been widely researched for use as conductive thin films and as forms of LSP. Bollavaram et al. [42] researched the use of metallic submicrofilms as LSP on

thermoset CYCOM-5320-1 prepreg composites with a total of 14 plies. They used two layers of NB-120 adhesive film that were applied to the composite substrate before the 10 mil thick LSP submicrofilms were applied. The panels were then post cured at a hold temperature of 120°C for three hours. Consolidated panel resistance measurements showed averages for gold, copper, aluminum, silver and pristine composite to be 0.51 Ω, 0.08 Ω, 0.02 Ω, 0.08 Ω and 20.29 Ω, respectively. Panels were tested at a Zone 1A lightning strike level of 200 kA. First a pristine carbon fiber panel was tested at Zone 1A and received no damage to the inside of the panel. The aluminum microfilm panel test at Zone 1A, shown in Figure 9, received damage on the back of the panel. All other metallic submicrofilms were free from back-side damage.

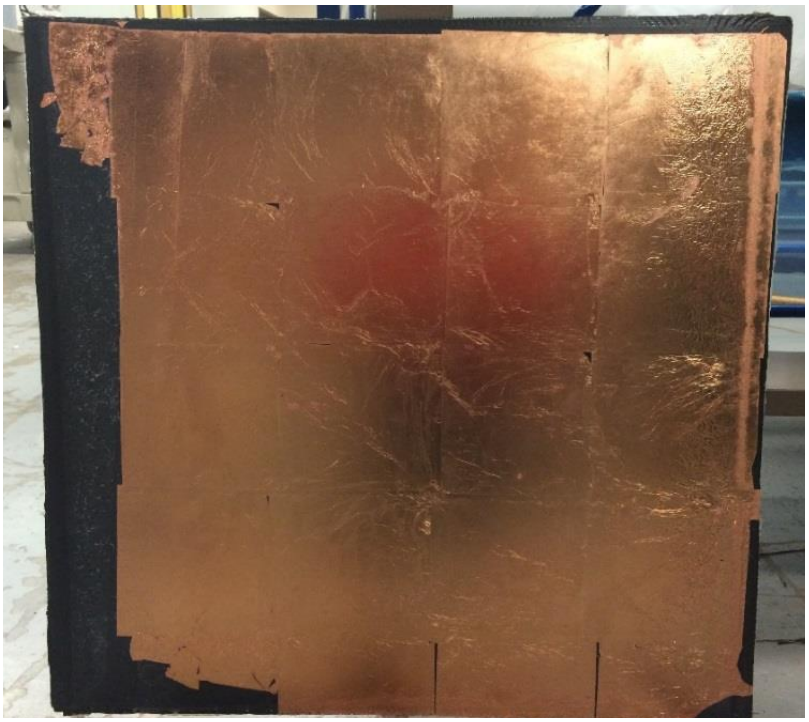

Figure 9. Composite panel with copper submicrofilm LSP [42].

Rathmell et al. [43] synthesized copper nanowires in an aqueous solution for use in transparent conducting films. NaOH (2000 mL) and $Cu(NO_3)_2$ (100 mL) were combined with EDA (30 mL) and hydrazine (2.5 mL) to produce 1.2 g of CuNWs which were stored in the

hydrazine solution in an argon atmosphere to prevent oxidation. Dimensions of the synthesized CuNWs were 90 nm in diameter and 10 μm in length. Dispersion was necessary for the as-produced CuNWs. This was achieved by sonication in 1 wt% polyvinylpyrrolidone (PVP) and 3 wt% hydrazine. Dispersed CuNWs remained suspended in the solution and were removed by filtration process, then transferred from the filter paper onto a 0.6 μm thick adhesive layer. Electrical percolation was achieved at 350 mg/$m^2$of nanowire density. The researchers reported a sheet resistance of 15 ohms/sq with 75% light transmittance.

Won et al. [44] synthesized CuNW transparent conductors for photovoltaics using an annealing free process. They utilized a simple aqueous solution using $CuCl_2*2H_2O$ (50 mg), hexadecyclamine (280 mg), and dextrose (100 mg) dissolved in water (20ml). The solution was placed in a vial and stirred at room temperature for an additional 12hrs, then capped with paraffin tape and heated in an oil bath at 100C for 6 hrs while stirring. The synthesized CuNWs were then washed three times with hexane and isopropyl alcohol (IPA). The purified CuNWs were stored in IPA to prevent oxidation. The CuNW dispersion was treated with (1 wt%) lactic acid, which removes both copper oxide and residual organics, before filtration through 1 um mixed cellulose ester filter paper. The resulting CuNWs, had an average length of 50 μm and an average diameter of 66 nm. Graphic results shown in Figure 10 illustrate the lowered contact resistance by removal of CuO_2 and capping agent and increased CuNW length (with respect to the work of Rathmell et al.).

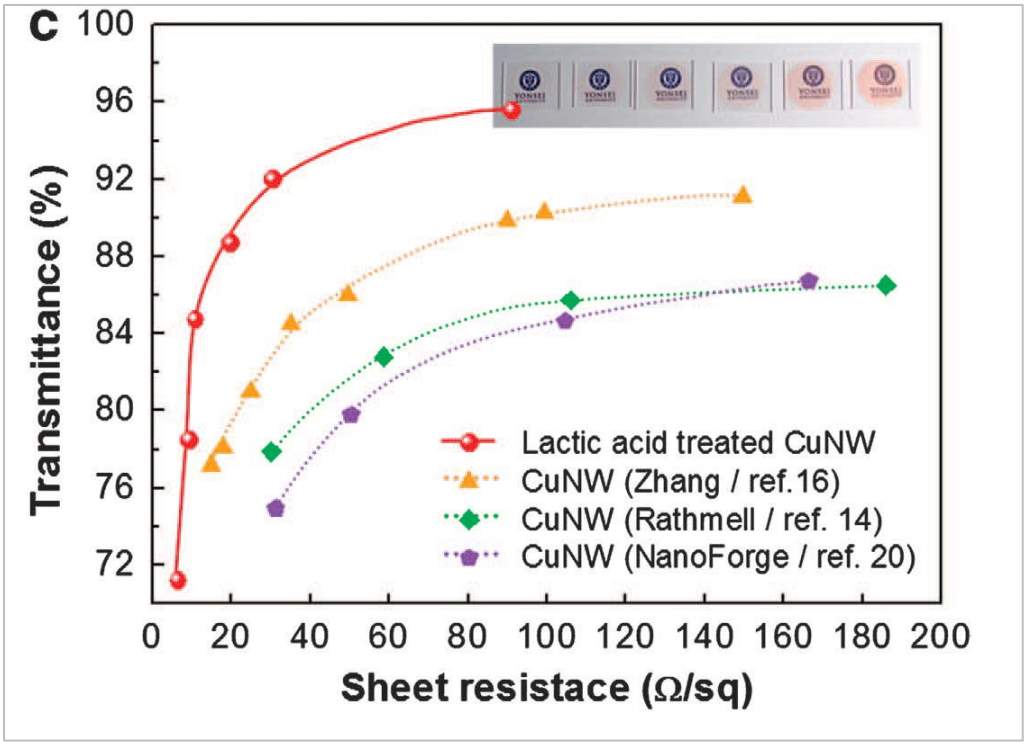

Figure 10. Transmittance vs sheet resistance for lactic acid-treated CuNW film, as compared to other references related to CuNW transparent electrodes [44].

Polavarapu et al. [45] conducted research on silver nanoparticle (NP) synthesis for printable electronics. PVP was used as a stabilizer in preparing a Silver NP ink. Silver nitrate (0.5 g) was reduced by slowly adding sodium borohydride (8 mL of 10 mg/mL solution) after dissolving with PVP (0.5 g) in deionized water. The solution was then stirred and filtered for purification. Excess PVP was removed by centrifugation. Then the NPs were stored in ethanol. The solution prepared with PVP resulted in silver NPs with diameters of 15-30 nm. The same preparation without PVP resulted in micrometer sized, insoluble powder, silver NPs. The dispersion was deposited onto polyethylene terephthalate (PET) substrates and sintered at only 50°C using a heat gun. The prepared thin films had a sheet resistance as low as 0.29 Ω/sq.

CHAPTER 3

EXPERIMENTAL MATERIALS AND EQUIPMENT

3.1 Materials

3.1.1 Thermoplastic Composite Test Panels

Each of the six test Panels are composed of Toray TC1225 unidirectional tape (Uni) LM-PAEK/carbon with a 16 layer quasi-isotropic, balanced-symmetric layup, autoclave processed and were generously donated by Triumph Aerospace Structures in Red Oak, Texas, as shown in Figure 11. Each panel was 20 in. x 20 in. square with an average thickness of 2.0 mm. Images of all test panels are available in Appendix A.

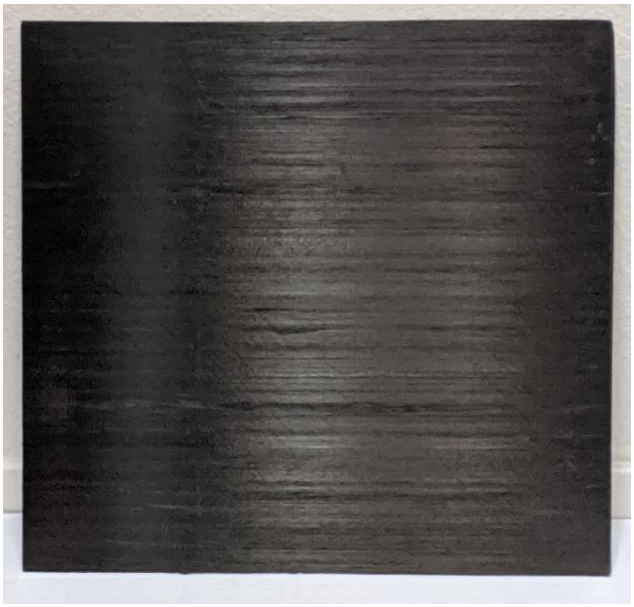

Figure 11. Toray TC1225 Uni, LM PAEK,
16 ply composite panel, 20 in x 20 in.

3.1.2 Nano and Sub-Micro Conductive and Dielectric Fillers

The following is a list of all of the conductive nano and sub-micro materials used in this study:

- Copper nanowires: Purchased from Skyspring Nanomaterials, Inc. in dry powder form, dimensions of minimum 5 µm in length and 300 +/- 100 nm in diameter.
- Graphene Platelet Nanopowder 0544DX (99.5 wt% carbon): Purchased from Skyspring Nanomaterials, Inc. in exfoliated dry powder form, with thickness of 11-15 nm and average particle diameter of 15 µm.
- Multi Walled Carbon Nanotubes (95wt% purity): Purchased from Cheaptubes.com, with dimensions of 8-15 nm in diameter and length of 10-50 µm, MWCNTs and synthesized by catalytic chemical vapor deposition (CCVD) and purified with concentrated acid chemistry.
- SilCoflake 93-102: Purchased from Technic, Inc. as mechanically flattened silver-coated copper flake, average particle diameter of 4.6 µm, specific surface area of 2.5 m/g. and containing 15 wt% silver (per datasheets provided by Technic).
- SilCoflake 93-104: Purchased from Technic, Inc. as mechanically flattened silver-coated copper flake, average particle diameter of 4.6 µm, specific surface area of 2.5 m/g. and containing 30 wt% silver (per datasheets provided by Technic).
- Hexagonal Boron Nitride: Purchased from MicroLubrol in powder form with a diameter of 0.5 µm.

3.1.3 Resin system for Conductive and Dielectric Matrix

- Epon Resin 8132: An epoxy bisphenol-A based resin purchased from Miller Stephenson.
- Epikure 3164: An oligomeric polyamine curing agent purchased from Miller Stephenson
- Epikure 3253: A tertiary amine, tris (dimethyl amino-methyl) phenol, was utilized as an accelerator, and purchased from Miller Stephenson.

The Epon Resin 8132, Epikure 3164, and Epikure 3253 were combined at a ratio of 100:125:3 respectively.

- Epon 815C, A bisphenol A based epoxy resin containing n-butyl glycidyl ether with low viscosity (500-700 cP), and purchased from Miller Stephenson.
- Epikure 3282 curing agent: A modified aliphatic amine adduct with moderate viscosity (2900-4900 cP), and purchased from Miller Stephenson.

The Epon Resin 815C and Epikure 3282 were combined at a ratio of 100:20.5.

3.1.4 Primer and Top Coat

The primer and top coat used in this study are as follows:

- Epoxy Primer: Sherwin Williams CM0481968, Sherwin Williams CM0110933, and Sherwin Williams, CM0120828.
- Top Coat: Sherwin Williams Y10942 White 7568 Topcoat Batch #629560, Sherwin Williams Admix CM0840A03, and Sherwin Williams Admix CM0840081.

3.2 Equipment

The equipment used in this study is discussed here.

3.2.1 Spray Equipment

A complete list of all painting equipment is available in Appendix B.

3.2.2 Characterization and Measurement Equipment

- Hirox RH2000 Optical Microscope: Microscope capable of 1500x magnification.
- Hioki RM3548 Resistance Meter. High-precision four-point measurement device for milli-ohms range resistance.
- Fluke 289 True RMS Multimeter: Equipment used in conjunction with a copper sheet resistance rig: (1in x 1in contact width by spacing length) for measuring ohms/sq.

- Analytical Balance: Digital lab precision scale with precision to 0.001 g.

3.2.3 LSP Coating Processing Equipment

Three dispersion instruments were used to disperse nanomaterials in the resin system in order to determine the one, or combination, best suited for preparation of well dispersed conductive networks at loading levels from 5 wt% to 80 wt%. After dispersions were drawn or sprayed, they were cured in a laboratory oven.

Thinky ARV-310 vacuum mixer: A planetary centrifugal mixer used for dispersion of solids in high viscosity liquids, and is capable of near-vacuum pressure during mixing in order to practically eliminate air bubbles within the mixture without the need for de-gassing (see Figure 12).

Figure 12. Thinky ARV-310 planetary centrifugal vacuum mixer.

Sonics VCX-130 PB Ultrasonic Processor: A 130 watt probe sonicator with a 6mm titanium alloy Ti-6Al-4V probe tip, operating at a frequency of 20 kHz (see Figure 13).

Figure 13. Sonics VCX-130 PBUltrasonic Processor [46].

Scilogex D500 Homogenizer: A shear mixer for low viscosity liquids with a rotor/stator configuration operating between 10,000 and 30,000 rpm (see Figure 14).

Figure 14. Scilogex D500 Homogenizer [47].

Laboratory Oven: The Thermo Scientific Thelco 6545 Precision Laboratory Oven, with a temperature range up to 200°C (see Figure 15).

Figure 15. Thermo Scientific Thelco 6545
Precision Laboratory Oven.

3.2.4 Lightning Strike Testing Equipment

Shown in Figures 16 and 17 are pictures of the direct effects of lightning (DEL) generator, control room, and test panel setup area. The lead-acid battery bank which provides the energy for the C bank, and the test fixture which holds the panel and transfers the current to the test panel and then to ground can be seen in Figure 16.

Figure 16. DEL test fixture behind fence with battery bank on yellow shelves in left background; capacitor room in right enclosure behind fenced area.

Figure 17. DEL test fixture and control room.

Figure 18 shows the test fixture with the calibration plate installed. Clamps which hold the test panel in place are electrically isolated from the test article with dielectric sleeves, visible

on the far right in Figure 18. The composite panel is placed over and clamped to the aluminum frame, which is electrically connected to ground.

Figure 18. DEL test fixture with aluminum calibration test article.

The probe, shown in Figure 19, is located 50 mm above the surface of the test article. A dielectric ball is attached to the probe so that the electrical arc does not directly attach to the panel. A thin copper wire is attached to the end of the probe and taped about four millimeters above the test article.

Figure 19. Zone 2A Setup with 20in. x 20in. test panel.

Table 1 lists the equipment used for the high-current direct effects of lightning generator testing.

TABLE 1

EQUIPMENT USED FOR HIGH CURRENT DEL TEST

Description	Manufacturer	Model Number	Serial Number	Cal Due Date
High-Current Generator	NIAR	HC1	001	N/A
Oscilloscope	Yokogawa	DL850E	91P313729	N/A
Analog Voltage Input Module	Yokogawa	701250	91P321170	N/A
Analog Voltage Input Module	Yokogawa	701250	91P321166	N/A
Current Monitor Probe, 1000:1, 500,000A	Pearson	1423	147997	N/A
Current Monitor Probe	Pearson	301X	147836	N/A
Current Probe 1:1500	Danisense	DS600IDSA	14170020014	N/A
Milli-Ohm Meter	Keithley	580	0685151	N/A

CHAPTER 4

EXPERIMENTAL PROCEDURE

4.1 Phase One: Dispersion and Electrical Resistance Trials

Phase One dispersion and electrical resistance trials are discussed in this section.

4.1.1 Nanomaterial Dispersion

A total of 77 trials were conducted to determine the two materials best suited for continuing to Phase Two for the spray-coating trials. The variables involved were mixing/dispersing equipment, time of mixing, speed of mixing, type of nanomaterial (including sub-micro materials), and wt% of nanomaterials with respect to total weight of mixture. Solvent content was also varied in order to reduce viscosity as necessary. A 2.25 in. x 3 in. x 1/8 in. substrate was prepared by sanding with 320 grit sandpaper and thoroughly cleaning with isopropanol until no residue remained on the rag. Initially the substrate was an aluminum plate coated with epoxy. This was changed to fiberglass after the first series of trials due to inconsistent readings with the aluminum. Later trials used thermoplastic composite as the substrate. The substrate was then offset by layers of (~30 μm thick) Kapton tape. The offset thickness was varied by stacking the tape in two to four layers (~60 μm to ~120 μm thick) to determine the effects of thickness on electrical resistance. All except two trial coupons were offset with three layers of Kapton tape.

The conductive LSP coatings were prepared initially using a five-step process. The steps were varied according to the dispersion method used. Three methods were initially tried: probe sonication, high-speed homogenizer, and Thinky Mixer.

- Step 1: The first step in the probe sonication method was mixing of the solvent, resin, and conductive filler. This was initially done by adding 5 g of resin to 5 g of solvent in a 25

mL beaker while stirring at 250 rpm on a magnetic stirrer for 15 min. Then the filler material was slowly added while the mixture was still stirring. As filler was added, it was necessary to increase the stirring speed, depending on the wt% loading of the conductive filler. After several trials, the order of mixing was changed. First, the conductive filler was added to the solvent until well stirred, then the resin was added, followed by continual stirring for 15 minutes. For the high-speed homogenizer, 5 g of resin was added to 150 mL of IPA and stirred for 15 min. Then the conductive filler was added while stirring as before. In preparation for the Thinky Mixer, 3 g of resin was added to each of the three containers designed to be placed in a carrier for this mixer. Then the nanofiller was added directly to the resin at the appropriate wt%. With this method, three trials could be processed at once.

- Step 2: In preparation for sonication, the mixture in the 25 mL beaker from Step 1 was placed in a water bath inside a 1000 mL beaker and held in position with a 3D printed jig so that it would not slip off center during sonication. Early trials were sonicated at a 60% amplitude for 45 minutes. Trials for CNTs varied the time from 30 min to one hour. Later trials were limited to 40% amplitude based on early results. In the high-speed homogenizer trials, the mixture was placed in a 500 mL flask and mixed at 18,000 rpm for 5 min. Thinky Mixer trials were run for 15 min at 2,000 rpm without the addition of solvent after an initial trial at 5 min and 2,000 rpm.
- Step 3: For the sonicated trials, the mixture was placed back on the magnetic stirrer until the viscosity increased until it was suitable for drawing on test coupons or for spraying. Initially, heat was applied at this stage to accelerate the evaporation of solvent. In later trials, no heat was applied out of concern for damage to the nanomaterials. The same

procedure was followed for the high-speed homogenizer. Solvent was added to the Thinky Mixer solids and stirred for 30 min.

- Step 4: Conductive filler solutions were removed from the stirrer, poured onto prepared TPC substrates offset with Kapton tape, and drawn across the surface with a 1/8-inch stainless steel rod.
- Step 5: Coupons were left out to cure at room temperature for various lengths of time and then placed into an oven to cure at temperatures ranging from 50°C to 130°C for varying durations to determine the temperature effects on resistance.

4.1.2 Microscope Characterization

Samples from various dispersion methods were placed on glass slides offset by Scotch tape (~30 μm thick) and covered with a cover-slide for viewing through a Hirox RH-2000 microscope set to 700x. Then they were placed on a light table, which allowed for viewing of the nanofiller material. Only low loading (10–35 wt%) samples were viewed until a determination could be made of the best dispersion method.

4.1.3 Electrical Resistance Characterization

Once dispersion methods were understood through trials and microscope viewing, the promising candidates were tested for electrical conductivity. Two resistance measurements were initially used to compare sheet resistance of the conductive coatings. The first was a four-point probe method using a Hioki RM3548 Resistance Meter. The second method measured sheet resistance using a surface probe. A rig, shown in Figure 20, was fabricated by 3D printing a glycol-modified polyethylene terephthalate (PETG) polymer frame to hold two 1 in. x 1 in. x ¼ in. copper plates parallel so that the distance between them was one inch.

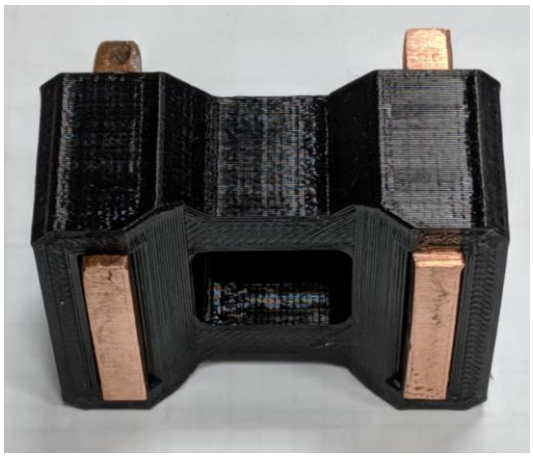

Figure 20. Sheet resistance rig with 1 in. square copper plates.

Copper electrodes were clamped to the positive and negative leads of a Fluke 289 Multimeter. Measurements were taken by placing the edges on top of the conductive film and reading the resistance, as depicted in Figure 21.

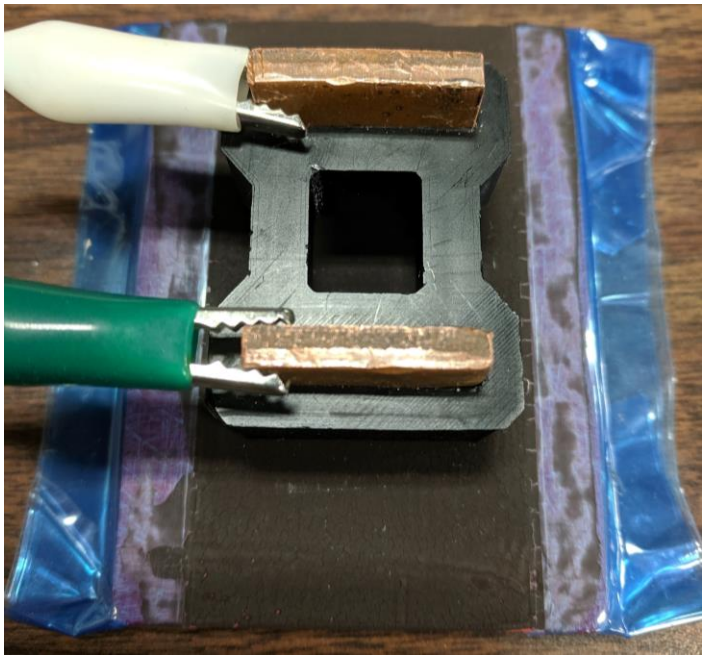

Figure 21. Sheet resistance rig with leads attached and placed on test coupon surface.

- Time Dependent Resistance: Once the conductive coating candidates had been narrowed down to only two, a representative set of samples was chosen to track changes in the

resistance over time. Coupons were measured for resistance over a four-week period to test for degradation of the conductive layer by oxidation or other causes.

- Resistance by Coating Thickness: Four samples were spray coated at various thicknesses to determine the impact of coating thickness on sheet resistance from the final conductive materials. Two drawn coupons were also created with two and four layers of 30 µm Kapton tape.

4.2 Phase Two: Lightning Strike Testing

Phase Two lightning strike testing is discussed in this section.

4.2.1 Test Article Preparation

Calculations for necessary materials by mass and volume were calculated based on the volume of material required to spray a 75 µm thick layer on a 20 in. x 20 in. panel, first by simply multiplying the panel area by the thickness and dividing by the expected percent loss of material during spraying. Material loss was determined during spray tests and is shown in equation (1).

$$Vol = (l * w * th)/L \quad (1)$$

where *Vol* is the volume of coating, *l* is the length of panel, *w* is the width of panel, *th* is the thickness of coating, and *L* is the loss during spray.

Next the density of the resin system was determined according to densities of the Epon 815C and Epikure 3282 and the mixing ratio of 100:20.5 prescribed in the Hexcel datasheets using equation (2).

$$\rho(Resin\ system) = 0.83 * \rho(815C\ resin) + 0.17 * \rho(3282\ curative) \quad (2)$$

where ρ is the density.

The wt% loading of the nanofiller and sub-micro filler materials was calculated by equation (3).

$$nano = (\%f * (R + C))/(1 - \%f) \quad (3)$$

where *nano* is the loading of nanofiller mass [g], $\%f$ is the amount of nanofiller by wt% (i.e. 0.20, 0.55, 0.70), *R* is the mass of resin [g], and *C* is the mass of curative [g]

Then, the necessary amounts of resin, curative and nanofiller were calculated by using GNU Octave programming language, which is provided in Appendix C

Six 20 in. x 20 in. panels were spray coated with the two most successful coatings based on the results of Phase One testing for resistance. This process took place over three consecutive days. On day one, the panels were first scuffed with 320 grit sandpaper, then carefully cleaned with isopropyl alcohol, and weighed individually. An aluminum plate was placed between panels for thickness measurements during each spray cycle. A dielectric coating was then spray coated on two panels with an HVLP Gravity Spray Gun. These panels were weighed again. Next, two panels with the higher wt% loading of conductive material 1 (CM1) and conductive material 2 (CM2) were individually spray-coated with the conductive coating at prescribed loading levels and again weighed.

On day two, the sanding, cleaning, and weighing of each of the four remaining panels was repeated as before. The two panels with and without HBN dielectric were spray coated with CM1 at 55 wt% loading, and the other two were spray-coated with CM2 at 55 wt% loading, as shown in Figure 22.

On the third day paint was spray coated after masking off a one-inch border for panel grounding during lightning strike testing. Figure 23 shows all six panels with borders masked

after conductive coat has been applied. The final top coat paint of approximately 125–150 μm is depicted in the image in Figure 24.

Figure 22. Two test panels being spray coated with Ag/Cu30 at 55 wt%: Panel on left sprayed with 20 wt% HBN dielectric coat, and panelon far right used to measure coating thickness.

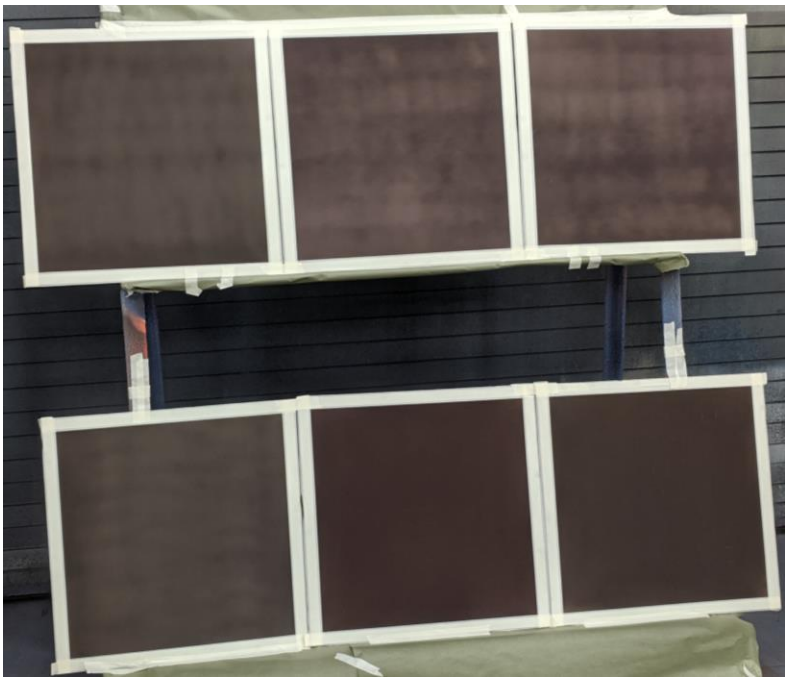

Figure 23. Six test panels with conductive coatings, with borders masked and ready for top-coat paint.

Figure 24. Six test panels with top-coat paint.

Dielectric coatings and conductive coatings were oven cured at 85°C for 18 hours and then applied to the six panels in the following manner (listed in the order of application to substrate):

- Test Panel 1:

  75 µm thick hexagonal boron nitride dielectric coat

  60–75 µm thick CM1 at 55 wt%

  125–150 µm thick primer and top coat

- Test Panel 2:

  No dielectric coat

  60–75 µm thick CM1 at 55 wt%

  125–150 µm thick primer and top coat

- Test Panel 3:

  No dielectric coat

  60–75 μm thick CM1 at 70 wt%

  125–150 μm thick primer and top coat

- Test Panel 4:

  75 μm thick Hexagonal Boron Nitride dielectric coat

  60–75 μm thick CM2 at 55 wt%

  125–150 μm thick primer and top coat

- Test Panel 5:

  No dielectric coat

  60–75 μm thick CM2 at 55 wt%

  125–150 μm thick primer and top coat

- Test Panel 6:

  No dielectric coat

  60–75 μm thick CM2 at 70 wt%

  125–150 μm thick primer and top coat

4.2.2 Lightning Strike Testing Procedure

Lightning strike testing was performed according to the standards set out in SAE ARP5416, Aircraft Lightning Test Method. Panels were placed on the aluminum-framed test fixture, where braided tinned-copper strips were folded around all four edges of the test article. Fiberglass plates were placed on top of the tinned-copper strips, and then clamps were closed over the plates to secure the test article and ensure good electrical contact between the aluminum frame and the test article. This procedure allows for current to flow out of the test panel to the

ground in any direction. A jet diverting electrode was situated 50 mm above the test article with an insulating ball attached to the end of the electrode. A copper initiating wire was attached to the electrode above the insulating ball by winding it several times around. The free end of the initiating wire was extended down towards the test article and attached to a piece of Scotch tape so that half of the tape was attached to the test article and the other half was bent upward. The initiating wire was then attached to the half of the tape which projected upward from the test article like a hinge, so that the end of the wire remained a few millimeters above the test article. The test setup, including the jet diverting electrode with copper initiating wire and insulating ball, is shown in Figure 25.

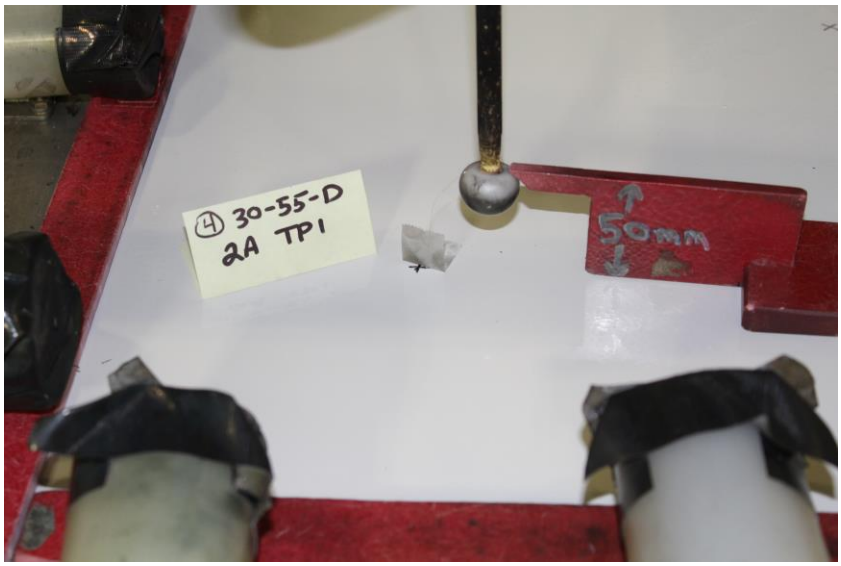

Figure 25. Jet-diverting electrode with insulating ball and copper initiating wire setup according to SAE ARP5416, Aircraft Lightning Test Method.

4.2.3 Test Levels

Testing was designed based on the requirements from ARP 5412, Revision B "Aircraft Lightning Environment and Related Test Waveforms," as shown in Table 2. This testing is for Aircraft Zone 2A which used current components D, B, and C*. Current component H was not necessary for this testing because its primary purpose is for the

Multiple Burst Waveform Set to test susceptibility of systems to multiple induced transients.

The requirements for the Aircraft Zone 2A current components are listed in Tables 3 and 4.

TABLE 2

APPLICATION OF LIGHTNING ENVIRONMENT TO AIRCRAFT ZONES

Aircraft Zone	Voltage Waveforms(s)	Current Component(s)
1A	A, B, D	A, B, C*, H
1B	A, B, D	A, B, C, D, H
1C	A	A_H, B, C*, D, H
2A	A	D, B, C*, H
2B	A	D, B, C, H
3 (Conducted)	-	A, B, C, D, H
3 (Direct attachment for new or novel designs- refer to 6.4.1)	A	A/5, B, C*
Lightning Strike Model Tests	C	

TABLE 3

HIGH-CURRENT WAVEFORM REQUIREMENTS FOR COMPONENTS A AND D

ARP 5412B: High-Current Waveform Requirements		
	Component A	**Component D**
Peak Amplitude	200kA ±10% 180–220 kA	100kA ± 10% 90–110 kA
Action Integral	2M A^2s ± 20% 1.6M–2.4M A^2s	250k A^2s ± 20% 200k–300k A^2s
Total Time Duration	< 500 µsec	< 500 µsec
Rise Time to 90% of Peak	< 50 µsec	< 25 µsec

TABLE 4

HIGH CURRENT WAVEFORM REQUIREMENTS FOR COMPONENTS B AND C

ARP 5412B: High-Current Waveform Requirements		
	Component B	**Component C***
Average Amplitude	2kA ± 20% 1.6 – 2.4 kA	≥ 400A
Charge Transfer	10 C ± 10% 9 – 11 C	18 C ± 20% 14.4 – 21.6 C
Total Time Duration	5 msec ± 10% 4.5 – 5.5 msec	45 sec ± 20% 36 – 54 msec

CHAPTER 5

RESULTS AND DISCUSSION

5.1 Results Phase One: Electrical Resistance

Phase One results relative to electrical resistance are discussed in this section.

5.1.1 Dispersion Method Results

Viewing early samples with an optical microscope was useful for determining the effectiveness of various nanofiller dispersion methods up to about 30 wt% loading. The light transmitted well through the resin system. Even with the curing agent included and in a cured state, the resin system appeared as a reddish-brown translucent background. The 700x magnification provided resolution down to 5 μm. Agglomeration could be clearly viewed, and in the case of CuNW and Ag/Cu, individual rods and flakes could be identified. This was not the case with CNTs and GNPs, because the filler dimensions were below the highest magnification of the optical microscope. It was difficult to see whether two conductive nano-filler particles were actually making contact or simply overlapped in two-dimensional viewing but on different levels of depth. The viewing method did, however, suffice for cross comparison between the different dispersion methods. Figure 26 shows CuNWs at 10 wt% loading dispersed by the high-speed homogenizer for 5 minutes at 18,000 rpm. It can be seen that there is obvious agglomeration. This method was eliminated because it proved to be the least effective dispersion method.

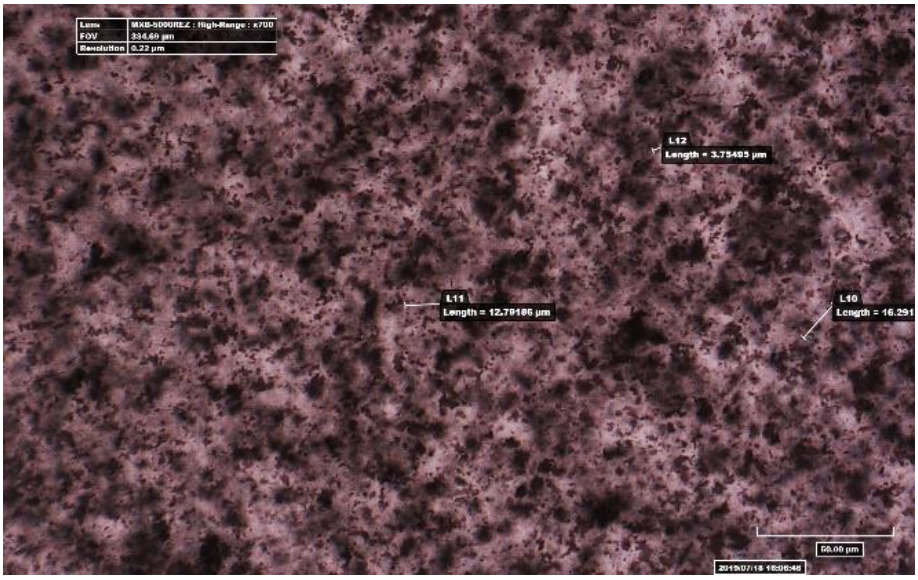

Figure 26. CuNW in epoxy matrix at 10 wt% loading dispersed by high-speed homogenizer for 5 min at 18,000 rpm. Scale bar = 50 µm.

The probe sonicator displayed the best results in terms of dispersion of CuNWs, as can be seen in Figure 27, as well as Ag/Cu flakes. However, images from the Thinky Mixer for CuNWs at 10 wt% at only 5 min of shear mixing at 1,500 rpm, shown in Figure 28, also proved to produce similar results at longer run times and higher rpm, even without the addition of solvent at high loading levels.

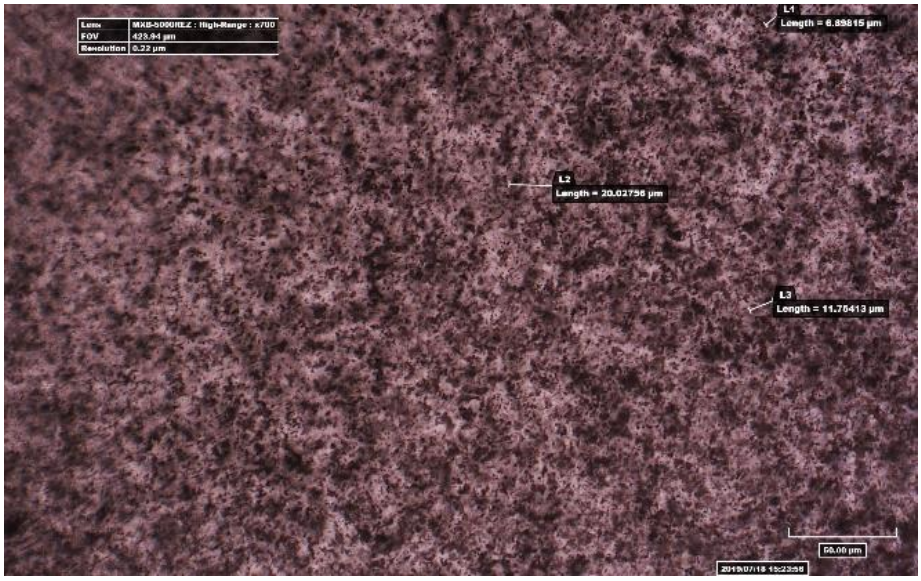

Figure 27. CuNW in epoxy matrix at 10 wt% loading dispersed by probe sonication for 60 min at 60% amplitude. Scale bar = 50 µm.

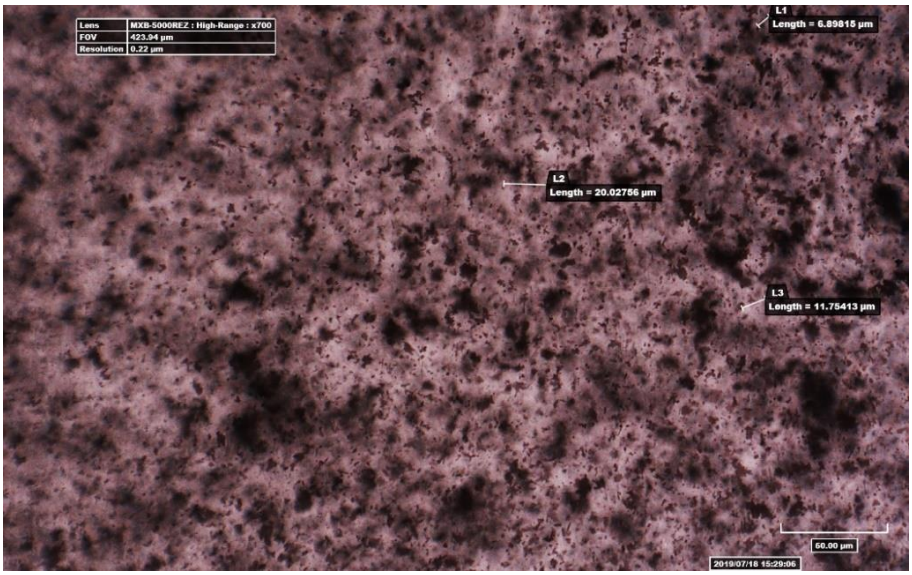

Figure 28. CuNW in epoxy matrix at 10 wt% loading dispersed by Thinky Mixer for 5 min at 1,500 rpm. Scale bar = 50 µm.

Figure 29 provides a detailed view, illustrating the lack of networked conductive Ag/Cu20 flakes. The image on the left appears networked, while the detail on the right shows the space between filler and lack of continuous path at 20 wt%. The appearance of blurry masses and masses with sharp edges indicates they are on separate focal planes.

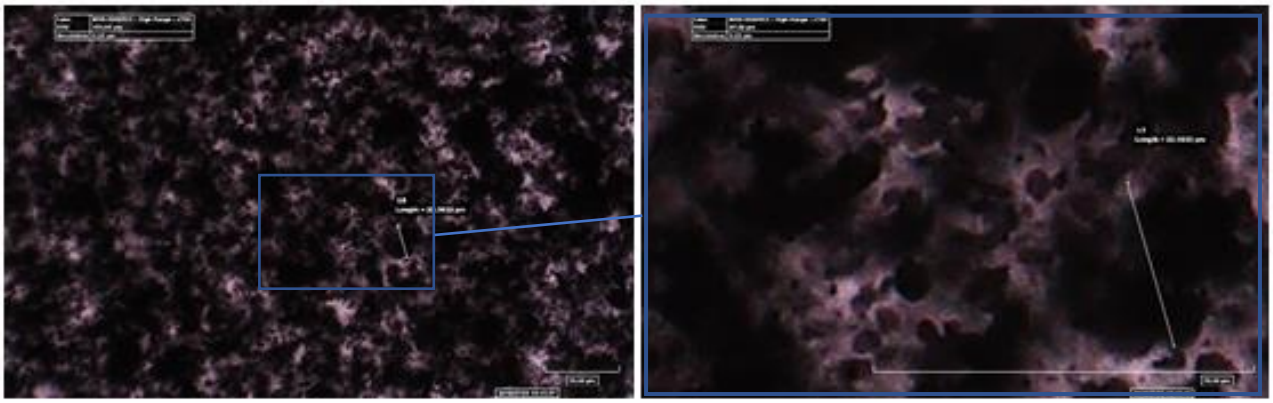

Figure 29. Ag/Cu flakes in epoxy matrix at 20 wt% (left) with detail (right) dispersed by Thinky Mixer for 15 min at 2,000 rpm. Scale bar = 50 µm.

Beyond approximately 35 wt% loading of conductive filler, optical microscopy becomes less effective since the light table below the particles no longer transmits light through the

material to the microscope lens. Figure 30 shows views lit from below (left) and above (right). One can see the beginning of networking of Ag/Cu flakes in the image on the left. The image on the right seems to be a continuous surface of solid filler. The 35 wt% loading level was the limit of the optical microscope and served the purpose of determining probe sonication as the best method for dispersion.

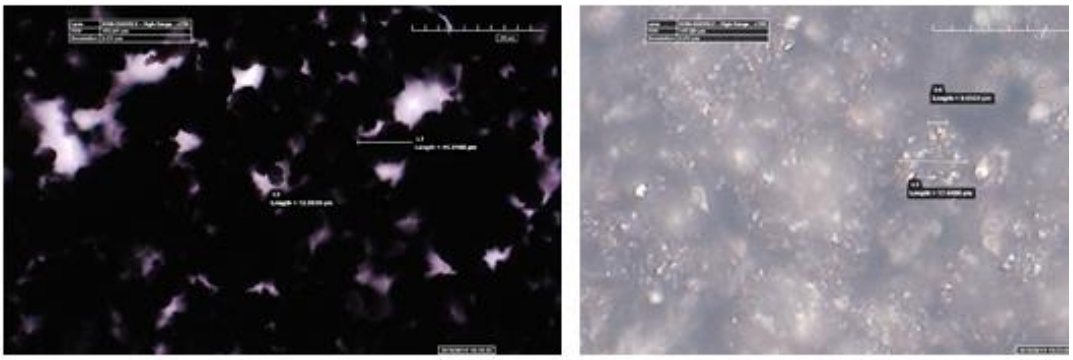

Figure 30. Ag/Cu flakes in epoxy matrix at 35 wt% dispersed by Thinky Mixer for 15 min at 2,000 rpm: bottom lit (left), and top lit (right). Scale bar = 50 µm.

5.1.2 Resistance by LSP Type

The combination of CNTs and GNPs was the first conductive material to be eliminated. Initial attempts to load 20 wt% of CNTs/GNPs at a 50:50 weight ratio resulted in a dry mixture that would overload the solution, producing either a thick paste that could not be drawn over the coupon, or a loose pulp when sufficient solvent was added. When manageable loading levels were attempted, up to 10 wt%, resistance was well above 250 Ω/sq, greater than the resistance of the bare TPC substrate.

Copper nanowires were the first material tested for conductivity. They were purchased and stored as a dry powder. Initial trials were conducted at low levels of conductive filler content below 10 wt% and up to 30 wt%. Aluminum plates were prepared with a 30 µm pure resin film before drawing the conductive nanofiller for the first 12 trials. At the time of the first dozen

trials, measurements were taken by sharp-tipped probes, and resistance measurements of 3 Ω to 6 Ω were recorded after 24 hours of curing. The resistance would steadily increase over time during measurement. Resistance measured over consecutive days also increased from one measurement to the next. The substrate was then changed to non-conductive fiberglass. All subsequent measurements were performed with the Hioki RM3548 Resistance Meter, and with the Fluke 289 Multimeter and sheet resistance rig. From this point forward, resistance measurements never fell below 2 kilo-ohms. Results for the CuNW trials are represented in Table 5.

TABLE 5

CUNW TRIALS

Trial No.	Nanomat'l	Wt%	Solvent	Dispersion Method	Time [min]	RPM or Level	Add'l Process	Resistance [kOhms/sq]
2	CuNW	9.1	Ethanol	Sonication	20	60%		N/A
3	CuNW	9.1	Ethanol	Sonication	40	60%		N/A
4	CuNW	9.1	Ethanol	Sonication	55	60%		N/A
5	CuNW	9.1	Ethanol	HSH	5	**10000**		N/A
6	CuNW	9.1	Ethanol	HSH	6	**18000**		N/A
7	CuNW	**3.9**	none	Thinky	5	1500		N/A
8	CuNW	**7.4**	none	Thinky	5	1500		N/A
9	CuNW	**10.7**	none	Thinky	5	1500		N/A
10	CuNW	10	Ethanol	Sonication	**20**	60%	Stir w/heat	N/A
11	CuNW	10	Ethanol	Sonication	**40**	60%	Stir w/heat	N/A
12	CuNW	10	Ethanol	Sonication	**60**	60%	Stir w/heat	N/A
13	CuNW	13.1	none	Thinky	10	2000	Thinky	N/A
18	CuNW	35	none	Thinky	15	2000	Thinky	N/A
19	CuNW	30	none	Thinky	15	2000		3.5
30	CuNW	40	none	Thinky	15	2000		400
31	CuNW	40	none	Thinky	15	2000		400
32	CuNW	40	none	Thinky	15	2000		400
34	CuNW	50	none	Thinky	15	2000		400
35	CuNW	60	none	Thinky	15	2000		400
79	CuNW	50	IPA	Sonication	30	40%	HVLP	400

Eventually all trials produced non-conductive results above 400 kilo-ohms. A test was set up where a PETG polymer block was 3D printed with a 3/16 in. x 1/4 in. cylindrical hole through the center. This block is shown in Figure 31. CuNWs were packed into the hole using the flat end of a solid stainless steel rod, and the Fluke 289 Multimeter probes were placed directly into each end of the hole to test for resistance. The resistance reading was in the mega-ohm range. An assumption was made that oxidation of the CuNWs had caused them to become non-conductive copper-oxides.

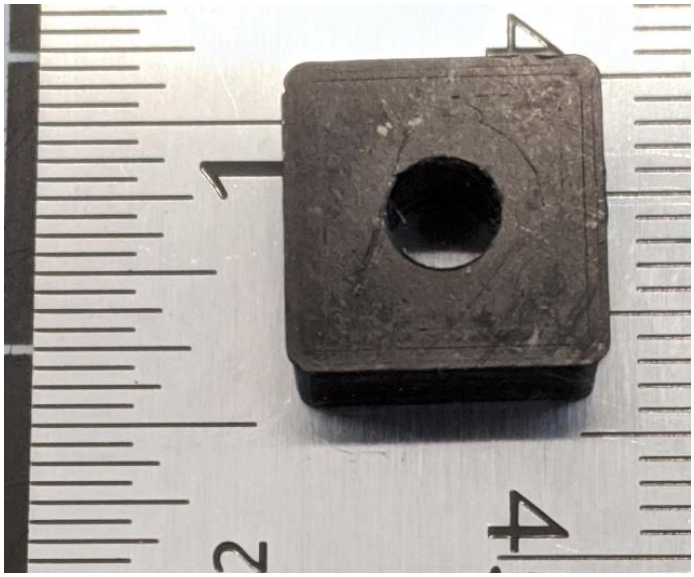

Figure 31. PETG block with 3/16 in. x 1/4 in. cylindrical hole for testing resistance of CuNWs.

Ag/Cu flakes at 35 wt% loading were the first trials to reach a percolation threshold resistance of 144 Ω/sq. As sonication methods were refined to include ratios of IPA close to 1:1 with respect to all solids, and stirring while sonicating, resistance levels were reduced. Loading levels of 50 wt% then began to result in single-digit sheet resistance values, as shown in Table 6.

TABLE 6

AG/CU TRIALS

Trial No.	Nanomat'l	Wt%	Solvent	Dispersion Method	Time [min]	RPM or Level	Add'l Process	Resistance [kOhms/cm]
14	Ag/Cu20	**9.1**	none	Thinky	15	2000	Thinky	N/A
15	Ag/Cu20	**13.1**	none	Thinky	15	2000	Thinky	N/A
16	Ag/Cu20	**16.7**	none	Thinky	15	2000	Thinky	N/A
20	Ag/Cu20	30	none	Thinky	15	2000		200
22	Ag/Cu20	40	none	Thinky	14	2000	Thinky	500
23	Ag/Cu20	35	**IPA**	Sonication/stir	45	60%	Stir w/heat	0.144
24	Ag/Cu20	35	**IPA**	Sonication/stir	45	60%	Stir w/heat	400000
25	Ag/Cu20	**80**	IPA	Sonication	30	60%	Stir w/heat	0.0015
26	Ag/Cu20	**40**	ethanol	Sonication	10	40%		0.05
27	Ag/Cu20	**40**	ethanol	Sonication	10	40%		0.05
38	Ag/Cu20	50	IPA	Sonication	30	60%	Stir w/heat	N/A
39	Ag/Cu20	50	IPA	Sonication	30	60%	Stir w/heat	0.017
41	Ag/Cu20	50	IPA	Sonication	30	60%	Stir w/heat	0.015
42	Ag/Cu20	50	IPA	Sonication	30	60%	Stir w/heat	0.012
43	Ag/Cu20	50	IPA	Sonication	30	60%	Stir w/heat	0.0015
44	Ag/Cu20	50	IPA	Sonication	30	60%	Stir w/heat	0.0015
48	Ag/Cu20	**50**	none	Thinky	15	2000		0.0035
49	Ag/Cu20	**50**	none	Thinky	15	2000		0.0085
50	Ag/Cu20	**50**	none	Thinky	15	2000		0.025
51	Ag/Cu20	50	none	Thinky	15	2000		0.028
52	Ag/Cu20	50	none	Thinky	15	2000		0.028
56	Ag/Cu-CNT	45-2	DMF	Sonication	45	40%		0.06
57	Ag/Cu20	55	IPA	Sonication	30	40%		0.003
58	Ag/Cu20	55	IPA	Sonication	30	40%		0.0075
59	Ag/Cu30	50	IPA	Sonication	30	40%		0.0033
60	Ag/Cu30	50	IPA	Sonication	30	40%		0.013
61	Ag/Cu30	60	IPA	Sonication	30	40%		0.0013
62	Ag/Cu30	60	IPA	Sonication	30	40%		0.003
63	Ag/Cu30	60	IPA	Sonication	30	40%		0.05
64	Ag/Cu20	60	IPA	Sonication	30	40%		0.0015
65	Ag/Cu20	60	IPA	Sonication	30	40%		0.0049
66	Ag/Cu20	70	IPA	Sonication	30	40%		0.0007
67	Ag/Cu20	70	IPA	Sonication	30	40%		0.0008
68	Ag/Cu20	70	IPA	Sonication	30	40%		0.0024
69	Ag/Cu30	70	IPA	Sonication	30	40%		0.001
70	Ag/Cu30	70	IPA	Sonication	30	40%		0.0013
71	Ag/Cu30	70	IPA	Sonication	30	40%		0.0016
72	Ag/Cu20	50	IPA	Sonication	60	40%		0.0021
73	Ag/Cu20	50	IPA	Sonication	60	40%		0.0028
74	Ag/Cu20	70	IPA	Sonication	60	40%		0.0017
75	Ag/Cu20	70	IPA	Sonication	60	40%		0.0011
76	Ag/Cu20	70	IPA	Sonication	60	40%		0.0009
77	Ag/Cu20	70	IPA	Sonication	60	40%		0.0008

Since the other two conductive coatings under consideration for lightning strike testing had been far too electrically resistive as prepared, a decision was made to include an alternative form of Ag/Cu flakes for the final test matrix. The Ag/Cu flakes originally included in the test matrix were copper flakes coated with 15%–20% silver by weight. Ag/Cu flakes with 30 wt% silver content was chosen to provide a comparison of relative silver content to determine whether the added cost of more silver provides any additional protection against lightning strike damage.

Ag/Cu conductive filler was processed by both the Thinky Mixer and by probe sonication. Trial 52 was the last one using the Thinky Mixer as a dispersion technique, because improvements in sonication processing were beginning to produce better results than the Thinky Mixer. Trial 52 compared the Ag/Cu20 mixed in the Thinky Mixer at 2,000 rpm for 15 minutes without solvent. The purpose of this trial was to determine whether mixing several small batches in advance of spray coating could be done over a series of days without the loss of conductivity due to higher viscosity of solvent-free mixing. Six samples were produced: two were applied immediately to test coupons, two were stored for two days in ambient conditions, and two were stored for four days in ambient conditions before application. Figure 32 shows the average increase in sheet resistance for the different storage times from immediate processing, processing after two days, and processing after four days: 3.5 Ω/sq, 16.5 Ω/sq, and 28.0 Ω/sq, respectively.

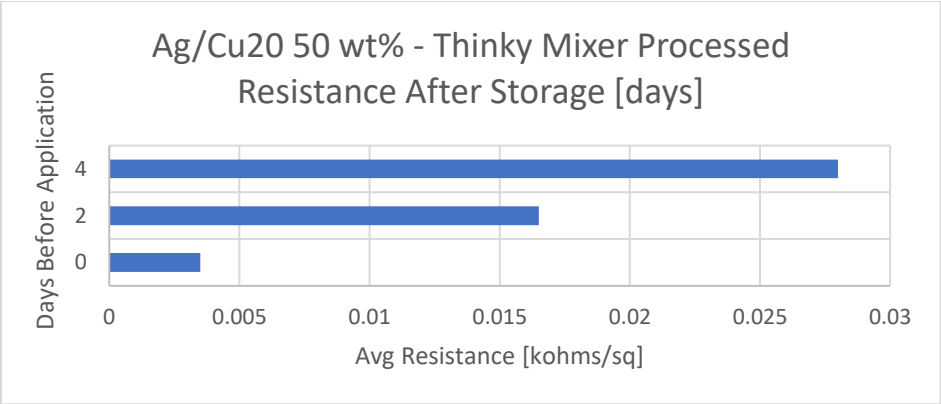

Figure 32. Ag/Cu20 post-mixing storage time (without curative) with respect to resistance.

This trial indicated that larger batches necessary for spray coating six 20 in. x 20 in. panels would have to be processed as needed, in order to remain properly dispersed for spraying over several days.

The trials immediately preceding the storage trial were performed by probe sonication in IPA and epoxy resin. The amplitude was set at 60% with a duration of 30 minutes with a programmed on/off power cycle set at two seconds on and one second off. The beaker was placed inside a larger water-filled beaker in order to absorb the heat energy produced by the sonication process. The two coupons processed for this trial both resulted in a sheet resistance of 1.5 Ω/sq. All trials after the storage trial were processed by probe sonication with an amplitude of 40% for 30 min. Trials with Ag/Cu30 were also begun at this point.

All resistance trials after trial 60 are shown in Figure 33. Ag/Cu20 resistance test coupons indicated a decrease in resistivity on samples up to 70 wt% loading, which resulted in a low resistance of 0.7 Ω/sq when sonicated at 40% amplitude for 30 minutes. Coupons loaded to 80 wt% after sonication at 60% amplitude for 30 minutes, returned a resistance of 1.5 Ω/sq, but cracked during curing once solvent was evaporated. Ag/Cu30 samples processed with the same sonication parameters as Ag/Cu20 returned less than 5% better average resistance values at 50 wt%, 60 wt%, and 70 wt%. At 55 wt%, the Ag/Cu30 value indicated by the solid blue diamond was taken from the large batch made for spray-coating the full-sized test panels. It was drawn onto a small TPC coupon by the same method as all other resistance test coupons. This value of 0.7 Ω/sq was equal to the lowest resistance from any sample tested at any loading level. The reason for this result is not clear, but may be attributed to use of a larger probe and a larger conductive coating batch. A small test coupon from the 55 wt% Ag/Cu20 large batch and the 70 wt% large batches were not produced due to scarcity of materials.

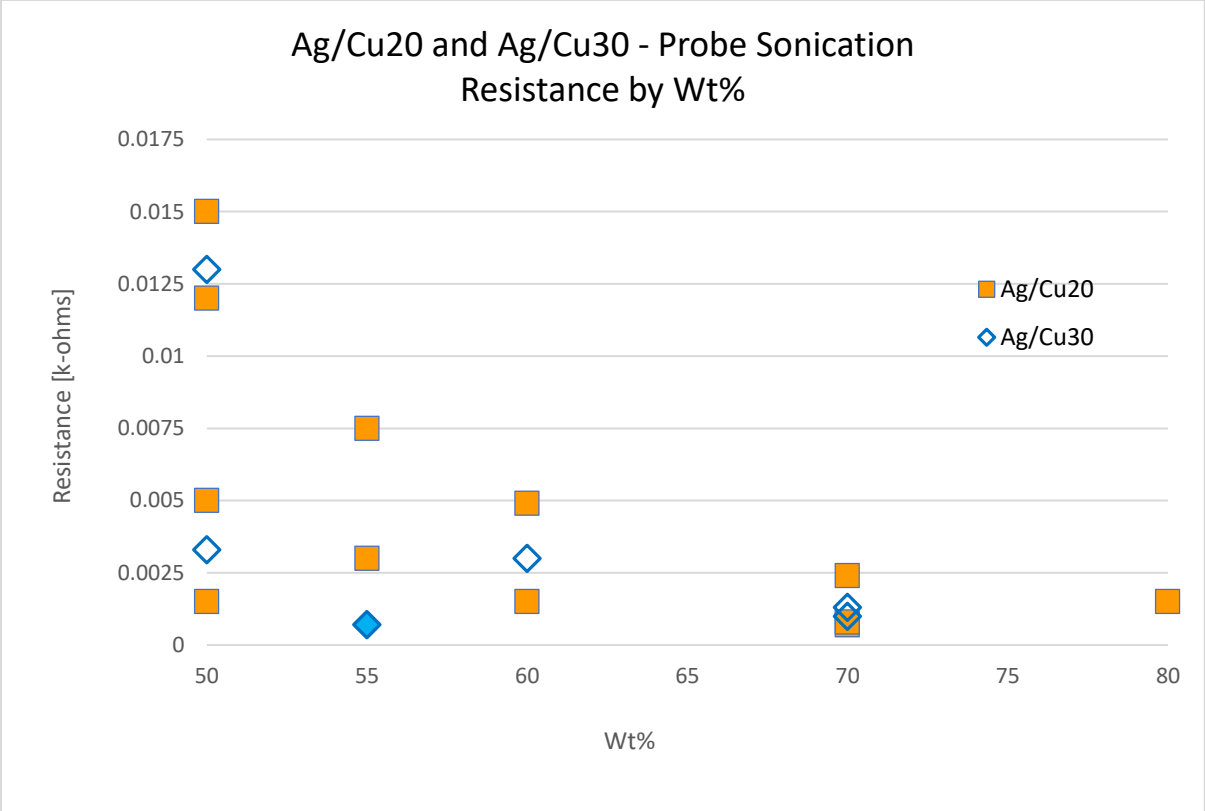

Figure 33. Ag/Cu20 and Ag/Cu30 sheet resistance results by conductive filler wt%. 50 wt% to 80 wt% by probe sonication. Blue filled diamond: drawn sample - final large panel spray batch.

5.1.3 Resistance by Coating Thickness

The second spray-coating test coupons were used to determine the effect of coating thickness on electrical resistance. Coupons were mounted on an aluminum plate before spraying with Ag/Cu20 at 70 wt%. The overspray around the coupons was measured with a Positector 6000 coating thickness instrument. Represented in Table 7, thicknesses of 20.3 µm, 28.2 µm, 37.3 µm, and 58.7 µm corresponded to resistance measurements of 1.7 Ω/sq, 1.0 Ω/sq, 0.9 Ω/sq, and 0.7 Ω/sq. Drawn samples were also made with three and four Kapton tape layers for cured thicknesses of 75 µm and 110 µm, with resistances of 0.8 Ω/sq and 0.7 Ω/sq, respectively.

TABLE 7

AG/CU20, 70 WT% SPRAY-COATING TRIAL
THICKNESS AND RESISTANCE

Ag/Cu20, 70 Wt% Spray Trial Coating Thickness & Resistance								
Panel	point 1	point 2	point 3	point 4	point 5	avg [mils]	avg [µm]	Resistance [Ω/sq]
1	0.6	0.5	0.6	2.0	0.4	0.8	20.3	1.7
2	1.9	1.3	0.8	0.9	0.9	1.1	28.2	1.0
3	1.1	1.7	0.8	2.2	1.6	1.5	37.3	0.9
4	1.4	2.3	1.8	2.5	3.6	2.3	58.7	0.7

This indicates thicknesses above 60 µm have little benefit in terms of conductivity. However, the different methods of application make a direct comparison invalid without additional characterization. In any case, the limit of resistivity never surpassed 0.7 µm on any Ag/Cu test coupon regardless of method of application or thickness. So, since too low a thickness had more detrimental consequences than too high, the decision was made to set the conductive spray-coating thickness for a range of to 60 µm to 75 µm in order to optimize the weight and resistance balance.

5.1.4 Change of Resistance with Time

Five Ag/Cu20 coupons were monitored for changes to sheet resistance over time. Resistance increased for the two Ag/Cu20 60 wt% samples by over 200%, while the remaining coupons only increased in resistance by less than 20%. The two panels which saw greater than doubling of the resistance were not oven-cured. The other three were cured within 24 hours of processing. The results are pictured graphically in Figure 34. The room temp cure time of the resin system is between four and seven days, about the time of leveling from the increase in resistance, suggesting Ag/Cu left in the uncured resin system tends to cause a change in the material which reduces conductivity whether it is by oxidation of the metal, or some other

means. This pattern was confirmed by measurements on other coupons, both room temperature cured, and oven cured.

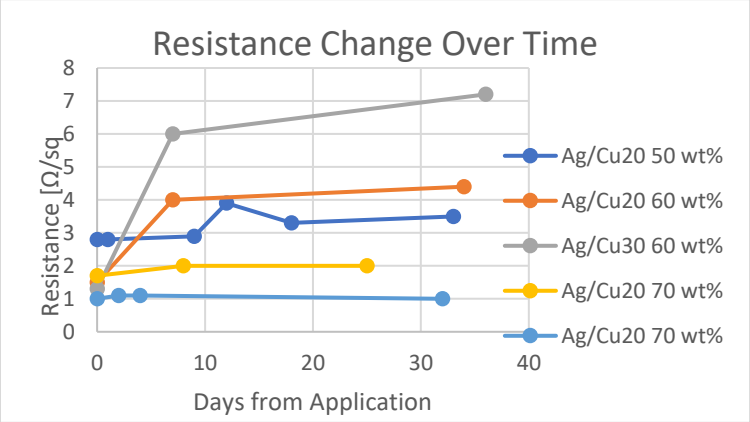

Figure 34. Ag/Cu change of resistance over time after application of conductive coating to substrate.

5.1.5 Final Test Matrix

The final test matrix is represented in Table 8. Each panel is large enough to be struck twice by simulated lightning at Zone 2A, giving two data points per condition. Final wt% levels were set at 55 wt% and 70 wt%. Dielectric loading was determined to be 20 wt% based on research by Han et al..[26] The weight of conductive nanofiller listed in Table 8 does not include the weight of the resin system. It is a calculated value based on the volume of material required to spray a 75 µm thick layer on a 20 in. x 20 in. panel, detailed in Experimental Procedures.

TABLE 8

FINAL TEST MATRIX

Final Test Matrix							
Panel No	Nanofiller	Nano mass [g]	Conductive Thick [µm]	Nanofiller wt%	Dielectric Thick [µm]	Dielectric Filler	No of Shots
1	Ag/Cu Flake 20%	32.5	<75	55	75	boron nitride	2
2	Ag/Cu Flake 20%	32.5	<75	55	0	no dielectric	2
3	Ag/Cu Flake 20%	50.6	<75	70	0	no dielectric	2
4	Ag/Cu Flake 30%	32.5	<75	55	75	boron nitride	2
5	Ag/Cu Flake 30%	32.5	<75	55	0	no dielectric	2
6	Ag/Cu Flake 30%	50.6	<75	70	0	no dielectric	2

5.1.6 Pre-test Panel and Coating Measurements

Final test panels were weighed for HBN dielectric and Ag/Cu conductive content and then areal weight was calculated for comparison to commercially available LSP. Common areal weights for expanded copper foil lightning strike protection (ECF) range from 73 gsm to 195 gsm. Areal weights for the 70 wt% Panels 3 and 6 were 87.2 gsm and 82.1 gsm respectively. This is slightly higher than the lightest, 73.2 gsm ECF that would be used on Zone 2A areas, and just over half of the more commonly used 142.5 gsm ECF for Zone 2A. This areal weight does not include the weight of any necessary LM PAEK which would be required to properly consolidate the ECF to a LM PAEK unitape composite surface. Panel weights, coating weights and areal weights for each coating on all six test panels are listed in Table 9.

TABLE 9

PANEL, DIELECTRIC, CONDUCTIVE COATING MASS, AND AREAL WEIGHTS

Panel and Coating Weights					
Panel No.	Bare Panel Wt. [g]	HBN Wt. [g]	HBN Areal Wt. [gsm]	Ag/Cu Wt. [g]	Ag/Cu Areal Wt. [gsm]
Panel 1	939.2	32.8	127.1	43.7	169.3
Panel 2	943.5	0	0	44	170.5
Panel 3	942.0	0	0	22.5	87.2
Panel 4	947.1	34.9	135.2	49	189.3
Panel 5	930.9	0	0	46.6	180.6
Panel 6	934.2	0	0	21.2	82.1

When resistance measurements were taken on final spray-coated lightning strike test panels, both Ag/Cu20 and Ag/Cu30 produced resistance levels between 0.6 Ω/sq and 0.8 Ω/sq. On the other hand, the Ag/Cu20 and Ag/Cu30 on final spray-coated lightning strike test panels averaged above 1.0 Ω/sq. Spray-coating of the Ag/Cu20 and Ag/Cu30 final test panels at 70% loading both appeared extremely rough in texture compared with the 55 wt% panels. The reason

for this result can be seen in post-test cross-section images taken from undamaged areas of the panels shown in Figure 35.

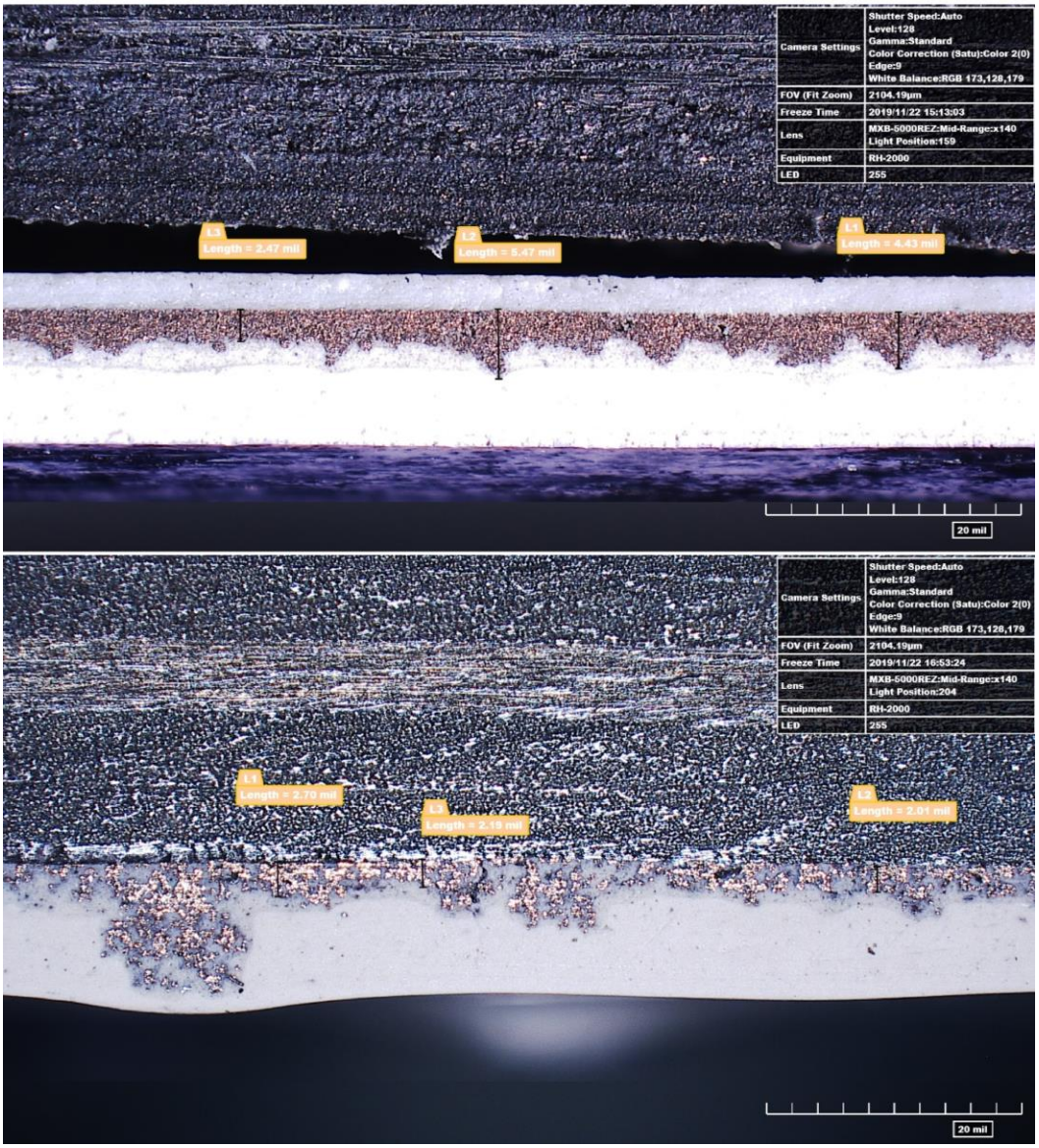

Figure 35. Cross-section micrographs from Panel 2 (Ag/Cu20, 55 wt%) (top) and Panel 3 (Ag/Cu20, 70 wt%) (bottom).

The spray-technician indicated that the high loading level of conductive filler, combined with high spray gun air pressure, may have resulted in a “dry spray”, which did not allow the flakes to lie flat on the surface of the panel. The bottom image in Figure 35 clearly shows the loosely packed, thin conductive layer of the 70 wt% Panel 3 compared to the 55 wt% Panel 2 in the top

of Figure 35. This loose packing was likely the cause of the higher than expected electrical surface resistance. Cutaway views of all other panels showed the same relative morphology between 55 wt% and 70 wt% panels.

Pre-spray viscosity measurements were not taken for dielectric or conductive coatings. Due to the limited amount of conductive material, there were only three preliminary spray-coating tests, and only one in which Ag/Cu at 70 wt% was used. The limited rehearsal and pre-spray viscosity measurement may have contributed to the increased roughness and resistance of the 70 wt% panels.

Coating thickness measurements were recorded for conductive coat, dielectric coat and top coat in three locations from each panel cross-section. Results are shown in Figure 36. Thickness measurements were taken from one small section of each panel, and so may not represent the overall thickness of the panels. Thickness of all 55 wt% panel conductive coatings was greater than the target by approximately 25%. The 70 wt% panel measured a 58 µm depth, about equal to the low end target. Irregularity of the conductive surface on Panel 6 prevented reliable measurements. Total paint thickness (primer + top coat) of all panels was greater, on average, than the target of 127 µm to 152 µm (5 to 6 mils), ranging from 142 µm to 222 µm (5.6 to 8.7 mils). All processing parameters are listed in the Experimental Methods section.

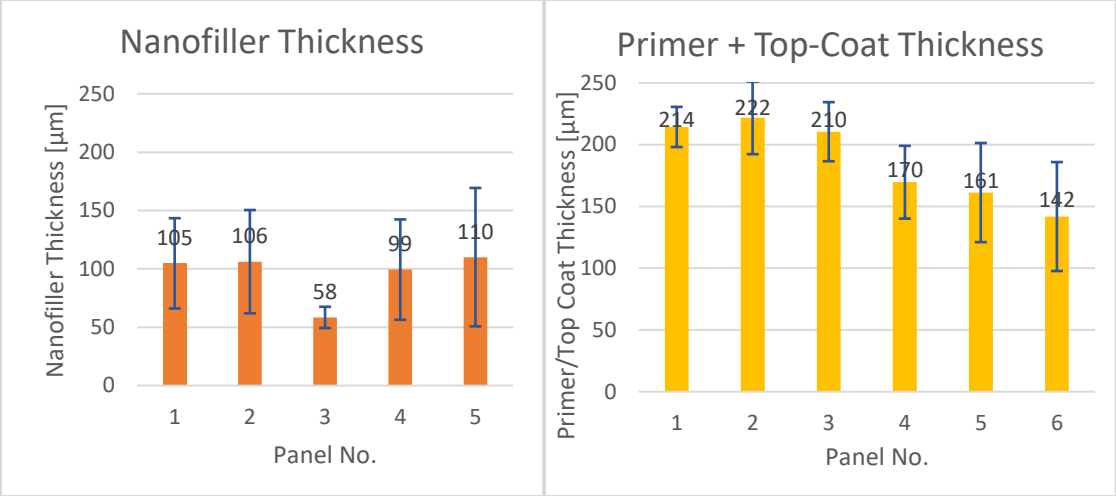

Figure 36. Nanofiller (left) and Paint Thickness (right) Measurements by panel number.

Pre-test images of the front and back of Panel 5 are shown in Figures 37 and 38. Pre and Post test images of all panels are provided in Appendix A.

Figure 37. Front of Panel 5 (Ag/Cu30, 55 wt%). Pre-test.

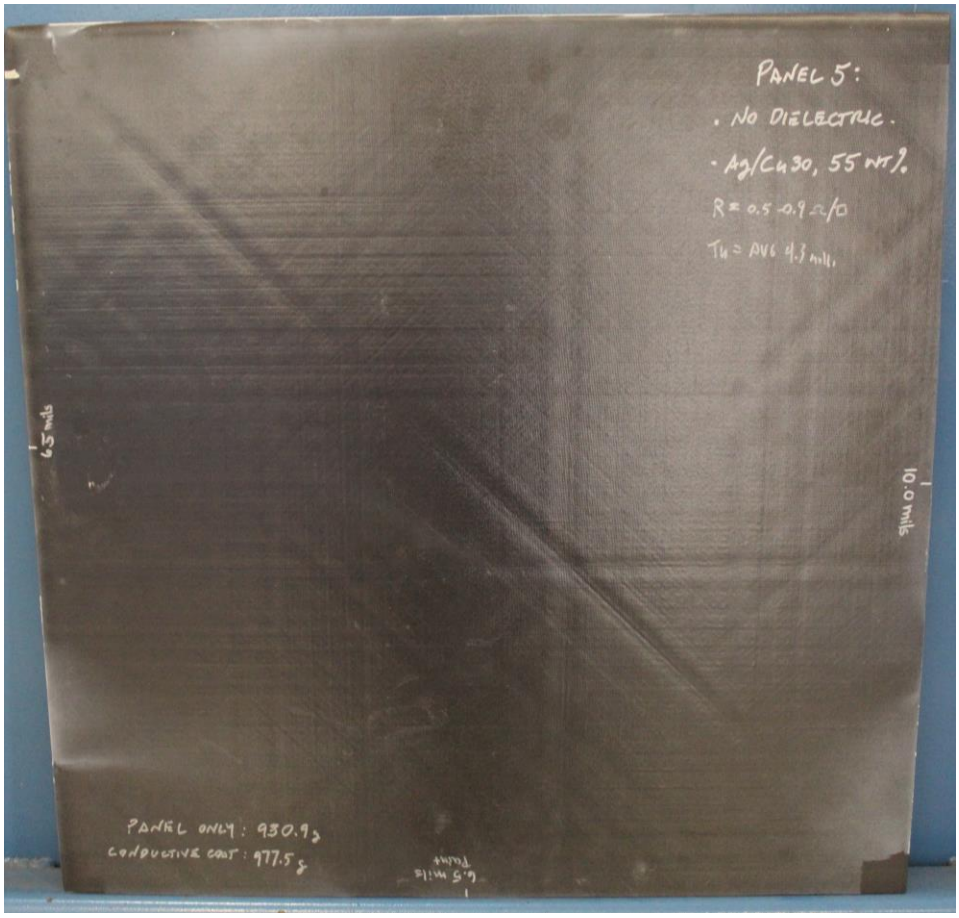

Figure 38. Back of Panel 5 (Ag/Cu30, 55 wt%). Pre-test.

5.2 Results Phase Two: Lightning Strike Testing

Phase Two results relative to lightning strike testing are discussed in this section

5.2.1 DEL Test Levels

All DEL generator testing waveform component data are listed in Table 10. Waveforms D, B, and C* were determined in accordance with SAE ARP 5412B, High Current Waveform Requirements listed in Tables 3 and 4. All test parameters were within ARP 5412B testing limits.

TABLE 10

DEL GENERATOR WAVEFORM TEST DATA FOR
HIGH CURRENT WAVEFORMS D, B, AND C

EUT	Test Point	Components	Component A/D				Component B			Component C/C*		
			Peak Amplitude (kA)	A/I	Rise Time (usec)	Duration (usec)	Average Amplitude (kA)	Charge Transfer (Coulombs)	Duration (msec)	Average Amplitude (A)	Charge Transfer (Coulombs)	Duration (msec)
Aluminum Panel	Waveform Verification	D, B, C*	-100.6	2.60E+05	8.4	160	2.12E+03	10.6	5	542.77	16.88	31.1
Panel 1 20-55-D	TP 1	D, B, C*	-103.53	2.40E+05	8.2	108	2.05E+03	10.25	5	403.61	22.53	55.82
Panel 1 20-55-D	TP 2	D, B, C*	-102.8	2.31E+05	8.4	103.4	2.05E+03	10.24	5	401.48	22.89	57.01
Panel 2 20-55	TP 1	D, B, C*	-102.6	2.28E+05	8.2	106	2.05E+03	10.26	5	418.28	22.38	53.5
Panel 2 20-55	TP 2	D, B, C*	-102.93	2.32E+05	8.4	105.2	2.04E+03	10.21	5	-0.67	0	0
Panel 3 20-70	TP 1	D, B, C*	-104.27	2.47E+05	8.2	117.8	2.06E+03	10.29	5	405.48	22.84	56.32
Panel 3 20-70	TP 2	D, B, C*	-104.53	2.48E+05	8.2	119	2.04E+03	10.2	5	391.59	23.47	59.93
Panel 4 30-55-D	TP 1	D, B, C*	-103.8	2.41E+05	8.4	110.4	2.01E+03	10.06	5	414.25	22.04	53.2
Panel 4 30-55-D	TP 2	D, B, C*	-103.67	2.42E+05	8.4	111.8	2.04E+03	10.19	5	387.28	22.97	59.32
Panel 5 30-55	TP 1	D, B, C*	-103.8	2.44E+05	8.4	116	2.03E+03	10.13	5	430.29	21.1	49.03
Panel 5 30-55	TP 2	D, B, C*	-104.07	2.42E+05	8.4	113.6	2.06E+03	10.3	5	429.57	21.16	49.26
Panel 6 30-70	TP 1	D, B, C*	-104.73	2.51E+05	8.4	120.6	2.04E+03	10.22	5	434.55	21.11	48.58
Panel 6 30-70	TP 2	D, B, C*	-104.67	2.51E+05	8.4	121.2	2.05E+03	10.27	5	428.53	21.39	49.91

Figures 39, 40, and 41 are graphic waveform data of the calibration tests performed on an aluminum test panel.

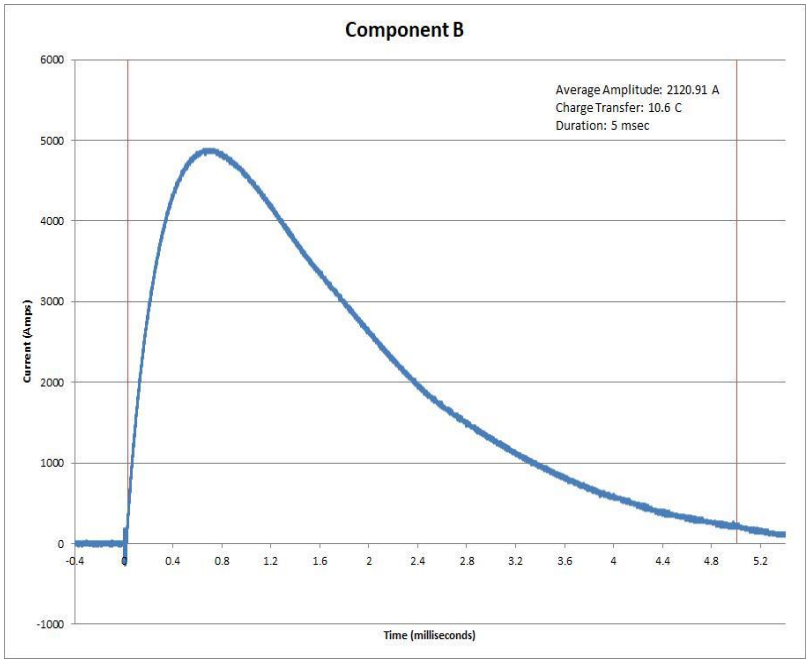

Figure 39. High Current Non-fuel Region – Waveform Verification – Zone 2A Component B.

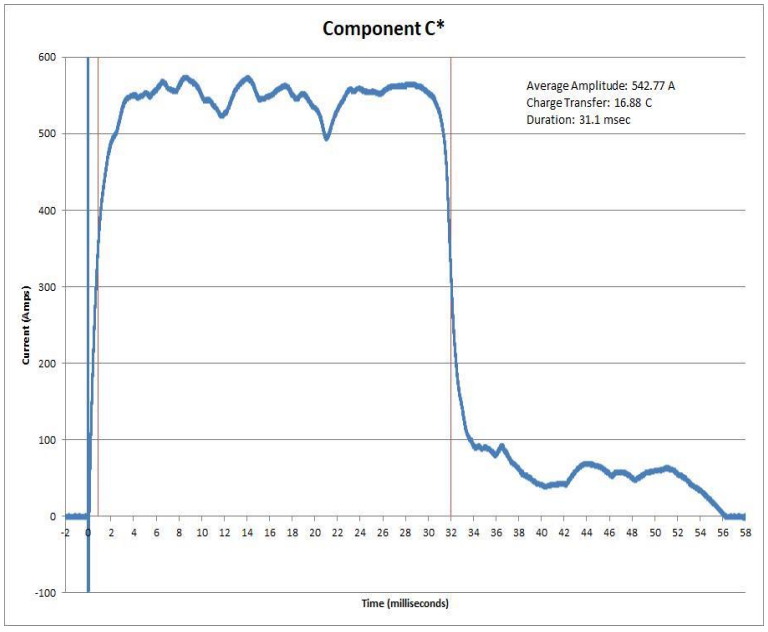

Figure 40. High Current Non-fuel Region – Waveform Verification – Zone 2A Component C*.

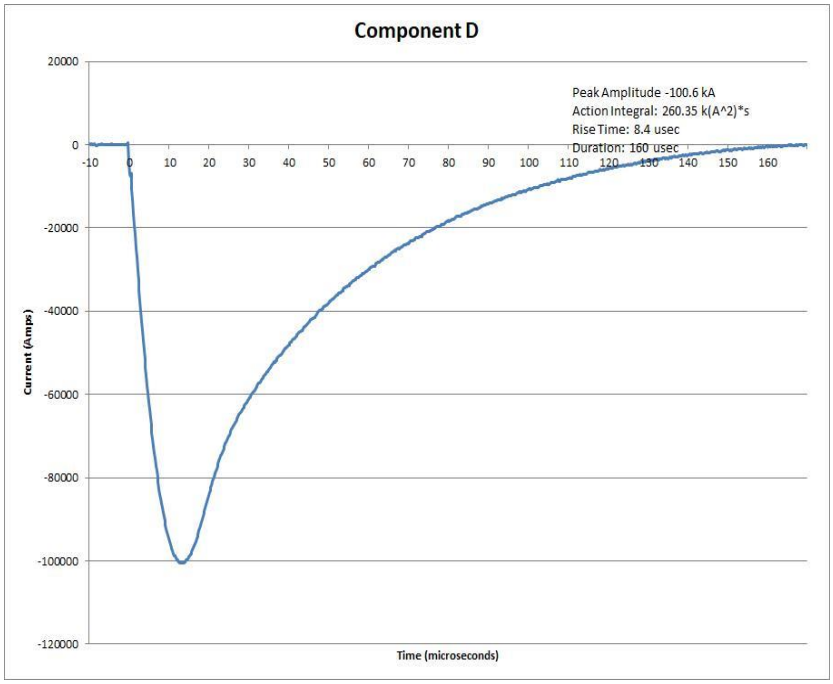

Figure 41. High Current Non-fuel Region – Waveform Verification – Zone 2A Component D.

5.2.2 Damage Criteria Definitions

Lightning strike damage was characterized by five main criteria:

- Outside Fiber damage – Outside of panel is painted side receiving the lightning current. Also denoted as front of panel. It is measured by the length of broken fibers between attachment endpoints to panel surface in the longitudinal direction. This value also equates to the majority of resin loss area. Transverse direction is measured by the width of all broken fibers. If more than one distinct area of broken fiber, as in the case of a split attachment or other isolated damage, each area is measured separately and totaled in the area calculation. Without considering delamination, it is rare for the fiber damage to plies below the surface to exceed the damage dimensions of the outer ply.
- Inside Fiber damage – Inside of panel is the bare carbon side facing away from the attachment of the lightning current. Also denoted as back of panel. It is measured by the

length of broken fibers between attachment endpoints to inner panel surface in the longitudinal direction. This value also equates to the majority of resin loss area. Transverse direction is measured by the width of all broken or damaged fibers. If more than one distinct area of damaged fiber, as in the case of a split attachment or other anomaly, each area is measured separately and totaled in the area calculation.

- Outside delamination – outside delamination is measured by "tap-test" using a heavy steel washer and tapping the outer surface of the panel while listening for a change of tone or deadening of the normal ringing response of the undamaged area of the panel as the washer nears the damaged area. This is performed in both the outer ply longitudinal fiber direction and the transverse fiber direction. This measurement equates to the de-bonding of one ply from the next and is more sensitive to plies near the outer surface ply. Outside delamination will also detect resin loss or fiber damage on the surface layer, as opposed to separation of one ply from the next without fiber damage which can happen between any two plies.
- Inside delamination – measured by the same method as Outside delamination but performed by tapping on the inside of the panels. This measurement also equates to the de-bonding of one ply from the next and is more sensitive to plies near the inner surface ply.
- Hole through panel – measured by the longitudinal and transverse size of hole fully penetrating through the panel. In terms of lightning strike, this is the most significant form of damage and therefore the one which LSP should be primarily designed to prevent.

In addition to discovering the most effective and efficient configuration of factors, several other direct comparisons to help determine the significance of each factor are discussed below.

5.2.3 Comparison of Silver Content

Three panels contain Ag/Cu20 conductive nanofiller in an epoxy matrix and three contain Ag/Cu30 in the same epoxy matrix. This allows a comparison between the content of silver coating on the copper flakes. Spray-coating target thickness for all conductive filler coatings was 60 µm to 75 µm. Actual coating thicknesses are discussed later in this section. The conductive nanofillers used in this study, Silcoflake 102 and Silcoflake 104, purchased from Technic Inc., are mechanically flattened copper flakes which are electrostatically coated with silver. Ag/Cu20 (Silcoflake 102) is sold as 15% to 20% silver, by weight. Ag/Cu30 (Silcoflake 104) is sold as 30% silver, by weight. The actual percent silver content of each batch is tested and provided to the customer in the datasheets. Data provided by Technic for this study indicated Ag/Cu20 and Ag/Cu30 were actually 15% silver and 30% silver, respectively. Panels 1 and 4 are both 55 wt% nanofiller, and both contain a 50 µm to 75 µm HBN dielectric layer. Figure 42 shows post-test pictures of the front (left) and back (right) of Panel 1. Figure 43 is post-test pictures of the front (left) and back (right) of Panel 4. Pre-test photos are provided in Appendix A.

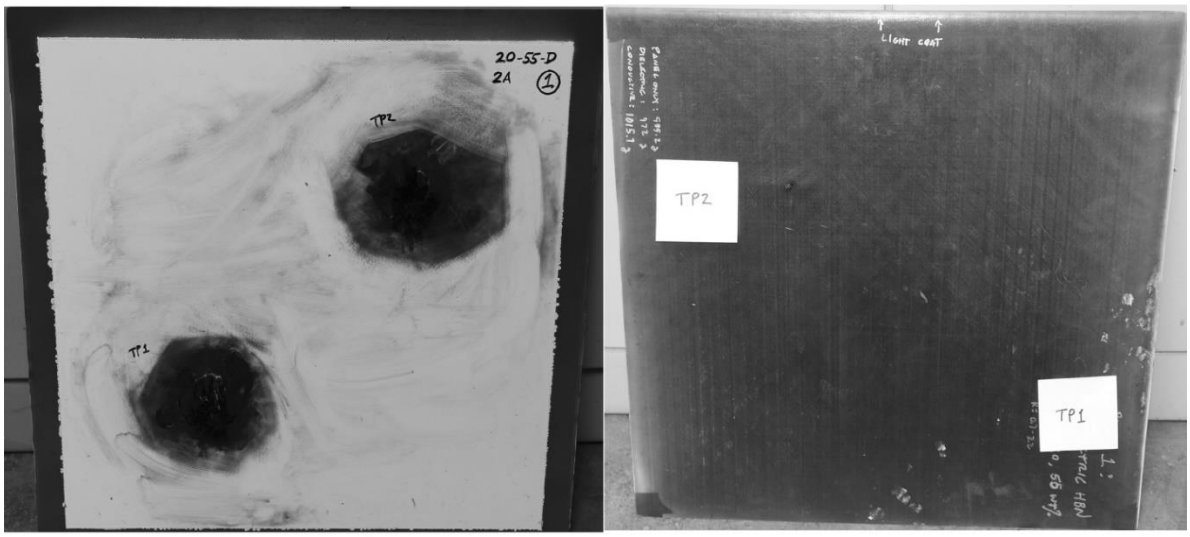

Figure 42. Panel 1 (Ag/Cu20, 55 wt%) with HBN dielectric. Front (left) and Back (right), Post-test (Residue was wiped from front panel surface).

Figure 43. Panel 4 (Ag/Cu30, 55 wt%) with HBN dielectric. Front (left) and Back (right), Post-test.

Using values from Table 11, the delamination values averaged by TP1 and TP2 on the front of each panel result in 5.93 in^2 for Panel 1 (Ag/Cu20), and 11.97 in^2 for Panel 4 (Ag/Cu30). It can be seen in Figure 43 (lower left of image) that Panel 4, TP1 had an isolated damage area in addition to the main attachment point.

In contrast, delamination area is larger on the back of Panel 1 (Ag/Cu20), TP2 than Panel 4 (Ag/Cu30), TP2 by almost 900% as seen in Figure 44. TP1 of Panels 1 and 4 did not exhibit any inside delamination.

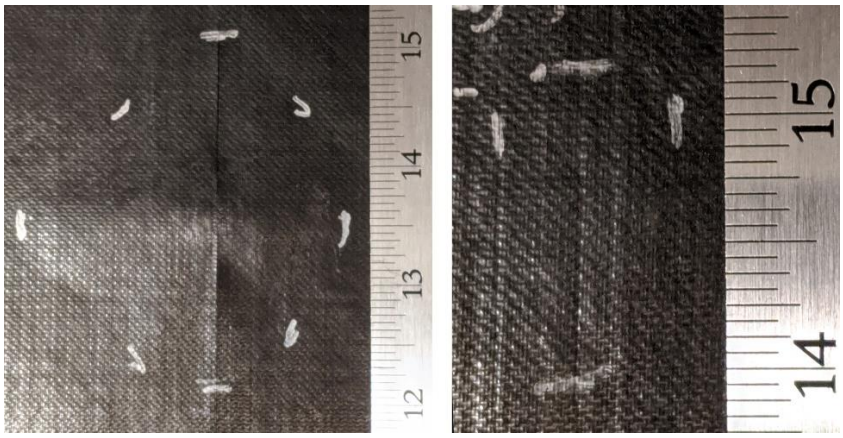

Figure 44. Post-test detail of Panel 1, TP2 (left) and Panel 4, TP2 (right). Inside delamination highlighted in silver marker for clarification.

TABLE 11

COMPARISON OF AG CONTENT BY SIZE OF DELAMINATION

					Delamination: Front			Delamination: Back		
Panel ID	Ag/Cu	Wt%	Dielectric Layer	Test Pt	Long.	Trans.	Area (sq/in)	Longitudin	Transverse	Area (sq/in)
1	20	55	D	1	2.5	2.25	5.625	0	0	0
1	20	55	D	2	2.5	2.5	6.25	3	2.75	8.25
4	30	55	D	1	3	3.25	9.75	0	0	0
4	30	55	D	1	3	1.75	5.25	0	0	0
4	30	55	D	2	3.25	2.75	8.9375	1.25	0.75	0.9375
2	20	55		1	3.25	2.5	8.125	11.5	1.5	17.25
2	20	55		1	1	1	1	0	0	0
2	20	55		2	3.25	4	13	1	2.75	2.75
2	20	55		2	0	0	0	0	0	0
5	30	55		1	4	2.75	11	0	0	0
5	30	55		1	0	0	0	0	0	0
5	30	55		2	3.75	3	11.25	0.25	0.5	0.125
3	20	70		1	3.75	5	18.75	0	0	0
3	20	70		2	3	3.2	9.6	0	0	0
6	30	70		1	4.25	3.25	13.8125	0	0	0
6	30	70		2	3	3.5	10.5	0	0	0

Panel 2 (Ag/Cu20, 55 wt%) without dielectric averaged 4.6 in^2 of outside delamination, while Panel 5 (Ag/Cu30, 55 wt%) averaged 11.1 in^2 outside delamination. Panel 2 (Ag/Cu20, 55 wt%), on the other hand, sustained more inside delamination, with TP1 receiving 17.25 $in^2$of

delamination while TP2 saw 2.75 in^2 on the inside. Its Ag/Cu30 counterpart, Panel 5, at TP2 received only 0.94 in^2 of inside delamination while TP1 received no delamination. The pattern of larger delamination on the front of the panels holds true for the 55 wt% panels with an HBN dielectric, as well as the 70 wt% panels.

The reason for the larger outside delamination of Panel 4 with less inside delamination than Panel 1 can be attributed to the better dispersion of resistive heat energy of the lightning current over the top of the panel with the Ag/Cu30 nanofiller, and therefore the temperature rise is less [12]. Research into the causes of delamination have shown panel deformation from the sudden explosive vaporization of the LSP and composite materials to be responsible in large part [48], [49]. It also stands to reason that if the polymer between plies retains its structure, more energy will be required to fracture the laminate. On the other hand, if the polymer, in this case LM PAEK, either melts or vaporizes, then less energy may be required to separate the lamina. Although a thermoplastic polymer matrix in its glass transition temperature region may be an exception worth further examination.

The combination of the high current density associated with the lightning channel along with the resistive heat generated can easily cause the temperature of the LSP and polymer to instantly exceed their pyrolization temperature. However, if the current can be quickly dispersed over the surface of the panel by a less resistive circuit, then less of the current's energy is concentrated in the more resistive composite, less Joule heat is generated in the material, and it is therefore less likely to reach its vaporization temperature. Since relatively less material is suddenly vaporized, including the LSP, there is also less explosive force to cause ply separation.

Fiber breakage occurs when the explosive forces of air breakdown, LSP vaporization, and resin vaporization, exceeds the tensile strength of the fiber bundles. Resin loss was almost

always associated with fiber breakage and is usually a prerequisite for any form of fiber damage, as LM PAEK is pyrolized above 600°C, well below the pyrolization temperature of the carbon fiber [4]. In this study, fiber damage was measured from the extent of detachment from the laminate where the resin was lost. This means that resin loss is included in the measurement but could potentially exceed fiber breakage where the fibers still adhere to the polymer of the next lower ply. In this study, however, the damage morphology was consistent, so that resin damage area and the extent of fiber detachment were equal, which is evident in Panel 2, TP1, shown in Figure 45.

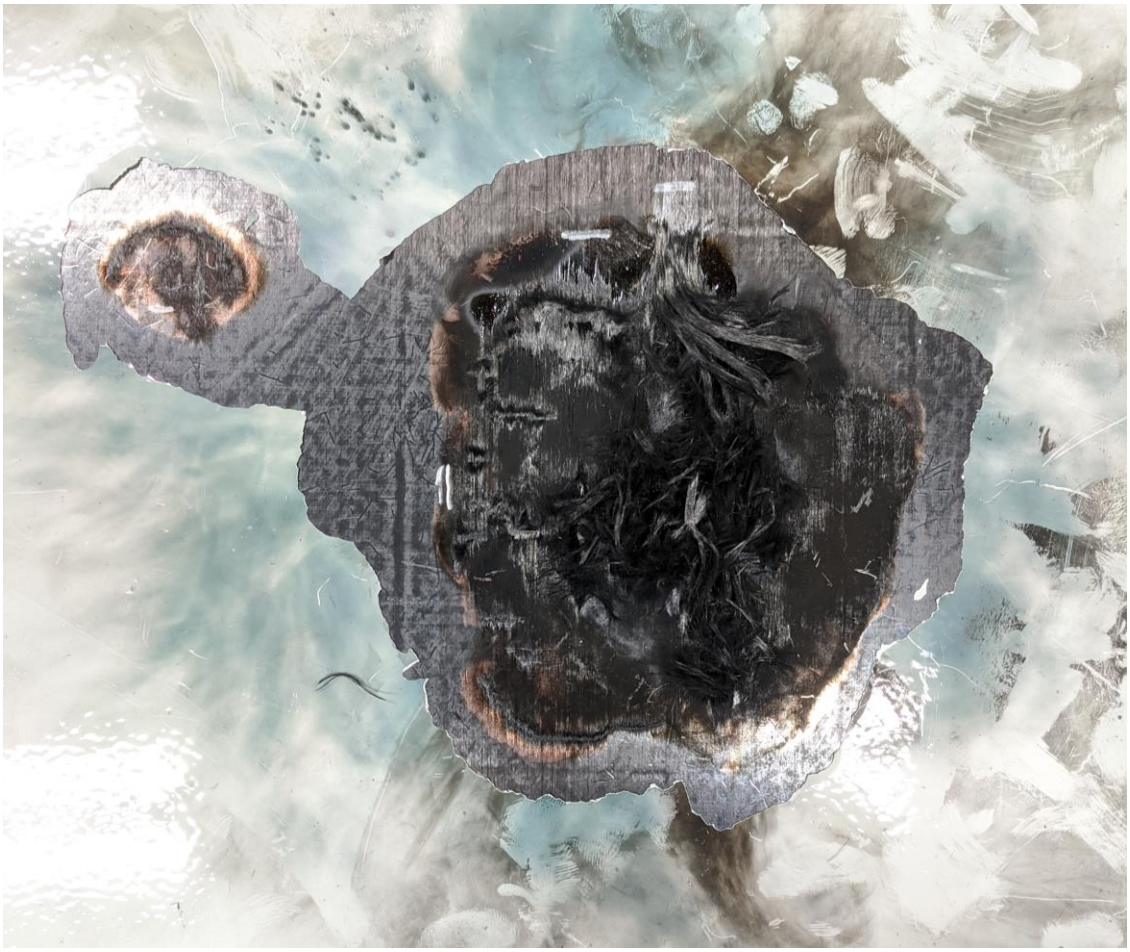

Figure 45. Panel 2 (Ag/Cu20, 55 wt%), TP1. Isolated damage areas - main area and island of less depth of damage. Paint has been peeled away for clarity of damage.

The fiber damage area is once again greater on the front of the panels for Ag/Cu30 than for Ag/Cu20, as it was for delamination area. The only test point to receive any fiber damage to the back of the panel was TP1 for Panel 2 (Ag/Cu20, 55 wt%) conductive filler and no dielectric, which stands out clearly in Table 12, although with an area of only 0.0625 in^2.

TABLE 12

COMPARISON OF AG CONTENT BY FIBER DAMAGE

Panel ID	Ag/Cu	Wt%	Dielectric Layer	Test Pt	Fiber Damage: Front			Fiber Damage: Back		
					Longitudin	Transverse	Area (sq/in)	Longitudin	Transverse	Area (sq/in)
1	20	55	D	1	2.25	1.75	3.9375	0	0	0
1	20	55	D	2	2	1.5	3	0	0	0
4	30	55	D	1	2	1.25	2.5	0	0	0
4	30	55	D	1	0.25	1.5	0.375	0	0	0
4	30	55	D	2	2.25	2.5	5.625	0	0	0
2	20	55		1	3	2.25	6.75	0.25	0.25	0.0625
2	20	55		1	0.125	0.5	0.0625	0	0	0
2	20	55		2	2.5	2.25	5.625	0	0	0
2	20	55		2	0.25	0.25	0.0625	0	0	0
5	30	55		1	3	2.5	7.5	0	0	0
5	30	55		1	0	0	0	0	0	0
5	30	55		2	2.25	3	6.75	0	0	0
3	20	70		1	2.75	3	8.25	0	0	0
3	20	70		2	2.75	3.5	9.625	0	0	0
6	30	70		1	4.25	3.25	13.8125	0	0	0
6	30	70		2	3	3.5	10.5	0	0	0

This same test point saw the largest inside longitudinal delamination of 11.5 in, as well, depicted in Figure 46.

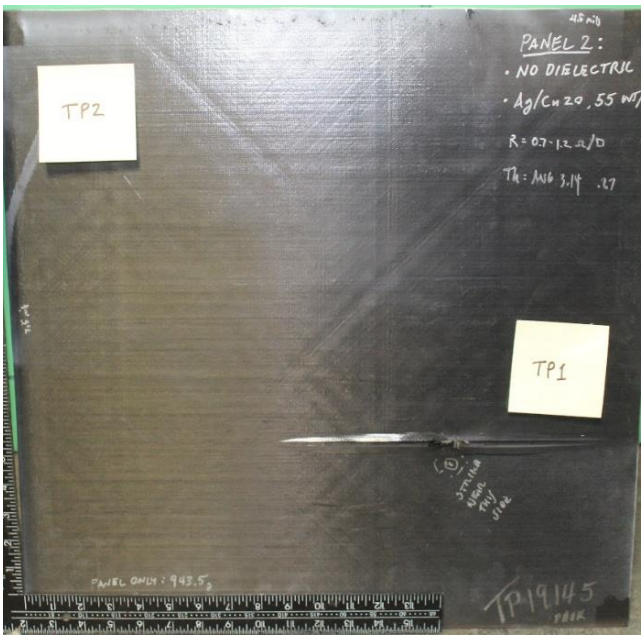

Figure 46. Back of Panel 2 (Ag/Cu20, 55 wt%), no dielectric. Fiber damage and delamination are seen at TP1. No Inside damage at TP2.

TP2 on Panel 2 was more in line with results for all other panels yet still received the third worst inside delamination. None of the other panels displayed any fiber damage on the inside. TP1 on Panel 2 was also the only panel to receive a hole through the panel, a detail of which can be seen in Figure 47. Though the hole was small, 0.25 in. x 0.125 in., this is damage considered most severe in terms of morphology since, depending on the location on an aircraft, it can lead to ignition of fuel vapors or disruption of electronic systems. Reasons for the disparate results between the two test points may be attributed to variations in paint thickness which, when thicker, could better contain the arc root, concentrating the energy of the strike. Thicker paint may also contain the vaporized LSP and resin, causing a more severe percussive deformation of the panel. It is well established that damage increases with increased paint thickness [7]. Since limiting the depth of damage is one purpose of LSP, the Ag/Cu30 protected the TPC more effectively than Ag/Cu20.

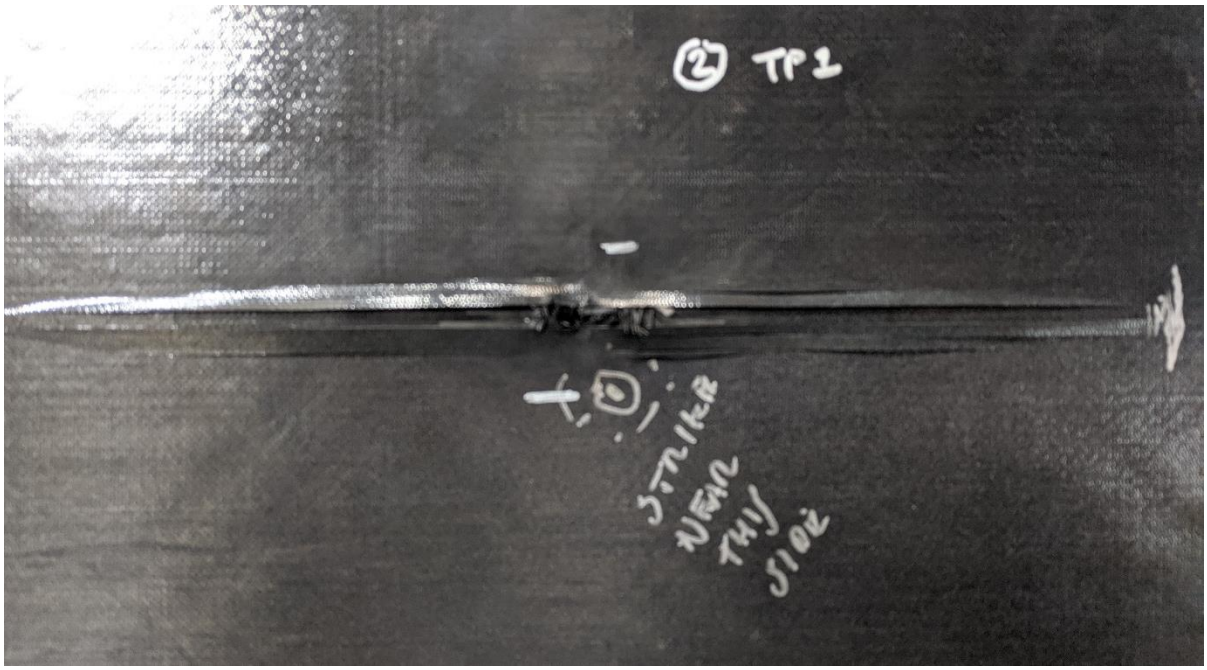

Figure 47. Close-up of inside delamination and hole on Panel 2 (Ag/Cu20, 55 wt%), TP1.

5.2.4 Comparison of Nanofiller Loading

The two nanofiller loadings were 55 wt% and 70 wt%. Nanofiller loading levels were chosen based on results from Phase One of this study. Loading levels above 50 wt% were chosen due to the reduce sheet resistance values. On average, sheet resistance values for drawn samples was higher than for sprayed samples, with 50 wt% coupons averaging 3.5 Ω/sq and sprayed samples averaging 1.5 Ω/sq. Sprayed samples sprayed with thickness above 60 µm were slightly more conductive than thinner films, but thicknesses above 75 µm did not show appreciable difference in conductivity. This trend was also found in drawn examples.

Mass of conductive coatings was discussed previously in Table 9, where the mass of both 70 wt% panels was found to be 22.5 g and 21.2 g, respectively. The coating mixtures for these two panels were processed completely separately; one with Ag/Cu20 and the other with Ag/Cu30. The four 55 wt% panel conductive coatings weighed 43.7 g. 44.0 g, 49.0 g, and 46.6 g, respectively. Despite this, and the fact that the 70 wt% panels both had higher resistance readings

of 2.3 Ω/sq and 2.4 Ω/sq, compared to the four 55 wt% panels with sheet resistance values of 0.7 Ω/sq, 0.7 Ω/sq, 0.6 Ω/sq, and 0.5 Ω/sq, neither of the 70 wt% panels received any delamination or fiber damage on the inside of the panel. If only the mass of the Ag/Cu is considered, the disparity in conductive coating mass is reduced. The averaged conductive nanofiller weight of the four 55 wt% panels is 45.8 g. The averaged conductive nanofiller weight of the two 70 wt% panels is 21.9 g. Rearranging equation 3, the mass of Ag/Cu can be extracted from the mass of polymer.

$$nano = \%f\ x\ ((R + C) + nano) \tag{4}$$

where $((R + C) + nano)$ is the total nanofiller weight of each panel.

The resulting conductive nanofiller average mass of 55 wt% panels is 25.2 g, while the average conductive nanofiller mass of 70 wt% panels is 15.3 g. While this closes the gap to 40% less nanofiller mass for the 70 wt% panels, it does not fully explain the better results by the 70 wt% panels. Table 13 displays the larger front side delamination areas, but this can again be attributed to better energy dispersion since the inside damage was less than their counterparts.

TABLE 13

COMPARISON OF DELAMINATION BETWEEN 70 WT% AND 55 WT% PANELS

					Delamination: Front			Delamination: Back		
Panel ID	Ag/Cu	Wt%	Dielectric Layer	Test Pt	Longitudinal (in)	Transverse (in)	Area (in²)	Longitudinal (in)	Transverse (in)	Area (in²)
2	20	55		1	3.25	2.5	8.125	11.5	1.5	17.25
2	20	55		1	1	1	1	0	0	0
2	20	55		2	3.25	4	13	1	2.75	2.75
2	20	55		2	0	0	0	0	0	0
3	20	70		1	3.75	5	18.75	0	0	0
3	20	70		2	3	3.2	9.6	0	0	0
5	30	55		1	4	2.75	11	0	0	0
5	30	55		1	0	0	0	0	0	0
5	30	55		2	3.75	3	11.25	0.25	0.5	0.125
6	30	70		1	4.25	3.25	13.8125	0	0	0
6	30	70		2	3	3.5	10.5	0	0	0

The fact that better surface energy dispersion equates to less damage through the depth is confirmed in terms of fiber damage, listed in Table 14. Averaging the two test points of each panel, the 70 wt% panels had 65% larger damage areas for Ag/Cu20 and 41% larger damage

areas for Ag/Cu30. None of the Ag/Cu 70 wt% panels had fiber damage on the back of the panels. Visual inspection of both 70 wt% panels shows several small “islands” of isolated damage. While this occured on at least one test point of every panel it is more pronounced on the 70 wt% panels. Figure 48 reveals the difference between the outside damage morphology between Panel 6 (Ag/Cu30, 70 wt%) (right), and Panel 5 (Ag/Cu30, 55 wt%) (left). Recalling Figure 35, where the cross-section of the 70 wt% panels showed large variations in nanofiller thickness suggests the unevenness of the coating thickness may have influenced results. It is possible that the proximity of the conductive nanofiller to the paint surface caused multiple leaders to reach up and distribute the arc root. The same micrographs from Figure 35 show the conductive nanofiller layer of the 70 wt% panel was closer to the surface than on the 55 wt% panel. Potentially there can be several of these leaders reaching up, dispersing the current density over a greater area of the panel, thus dividing the focus of the lightning strike energy. This could explain the consistently better results of the 70 wt% panels despite the nearly 40% less conductive material.

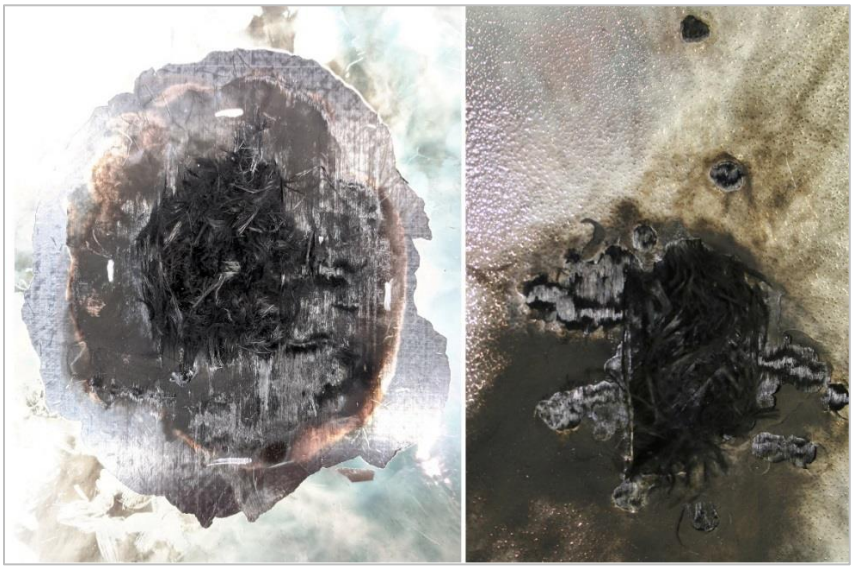

Figure 48. Outside damage morphology Panel 5 (Ag/Cu30, 55 wt%) (left) and Panel 6 (Ag/Cu30, 70 wt%) (right).

TABLE 14

COMPARISON OF FIBER DAMAGE BETWEEN 70 WT% AND 55 WT% PANELS

Panel ID	Ag/Cu	Wt%	Dielectric Layer	Test Pt	Fiber Breakage: Front			Fiber Breakage: Back		
					Longitudinal (in)	Transverse (in)	Area (in²)	Longitudinal (in)	Transverse (in)	Area (in²)
2	20	55		1	3	2.25	6.75	0.25	0.25	0.0625
2	20	55		1	0.125	0.5	0.0625	0	0	0
2	20	55		2	2.5	2.25	5.625	0	0	0
2	20	55		2	0.25	0.25	0.0625	0	0	0
3	20	70		1	2.75	3	8.25	0	0	0
3	20	70		2	2.75	3.5	9.625	0	0	0
5	30	55		1	3	2.5	7.5	0	0	0
5	30	55		1	0	0	0	0	0	0
5	30	55		2	2.25	3	6.75	0	0	0
6	30	70		1	4.25	3.25	13.8125	0	0	0
6	30	70		2	3	3.5	10.5	0	0	0

5.2.5 Comparison of HBN Dielectric to No Dielectric

No clear trend could be seen when comparing panels containing an HBN dielectric sub-layer to those without. Only the lack of a hole on either of the HBN dielectric panels separates the two panel types, while inside delamination was observed on both Ag/Cu20 and Ag/Cu30 panels. With limited data, no conclusive statement can be made with respect to effectiveness as a lightning strike protection layer. Without a clear performance benefit, the doubling of LSP areal weight with the HBN dielectric is a considerable drawback, given the high cost of mass in the commercial aircraft industry.

5.2.6 Conductive Nanofiller Cost Comparison

A spray-coated commercially available LSP utilizes an epoxy carrier with a silver sub-micro or nanomaterial-based filler. According to available documentation, the particle filler is nearly 100% silver content. The following calculations are based on the assumption that the commercially available conductive material of spray-coated sub-micro or nanomaterial LSP is 100% silver. The cost of copper bullion on September 20, 2019 was $0.19 per ounce. The cost of silver bullion was $18.44 per ounce on the same date. Table 17 provides the calculations of material costs for the individual metals used in the Ag/Cu20 and Ag/Cu30 nanofillers. Also

included are metals costs for Ag/Cu40 (40 wt% silver), Ag/Cu50 (50 wt% silver), and pure silver. Material cost for Ag/Cu20 is 20.84% of pure silver cost and Ag/Cu30 is 30.73% of pure silver cost, since the cost per ounce of copper is about 1% the cost of silver. A graphic comparison is provided in Figure 49.

TABLE 15

COST OF NANOFILLER PER KILOGRAM WITH RESPECT TO RATIO OF AG TO CU BY WT%.

	Ag/Cu20	Ag/Cu30	Ag/Cu40	Ag/Cu50	Pure Ag
Ag amount [oz]	6.4302	9.645	12.86	16.08	32.15
Cu amont [oz]	25.72	22.51	19.29	16.08	0
Total Wt. [oz]	32.1502	32.155	32.15	32.16	32.15
Ag cost/oz [$/oz]	18.114	18.114	18.114	18.114	18.114
Cu cost/oz [$/oz]	0.19	0.19	0.19	0.19	0.19
Ag cost [$]	116.4766	174.7095	232.946	291.2731	582.3651
Cu cost [$]	4.8868	4.2769	3.6651	3.0552	0
TOTAL Cost [$]	121.3634	178.9864	236.6111	294.3283	582.3651

Metal	*$/oz	*$/kg
Ag bullion	18.44	573.484
Cu bullion	0.19	5.909

*Based on price of Ag & Cu bullion on 9/20/2019

Note: Conversion rate used by Technic, Inc. 32.15 OZ. = 1 KG

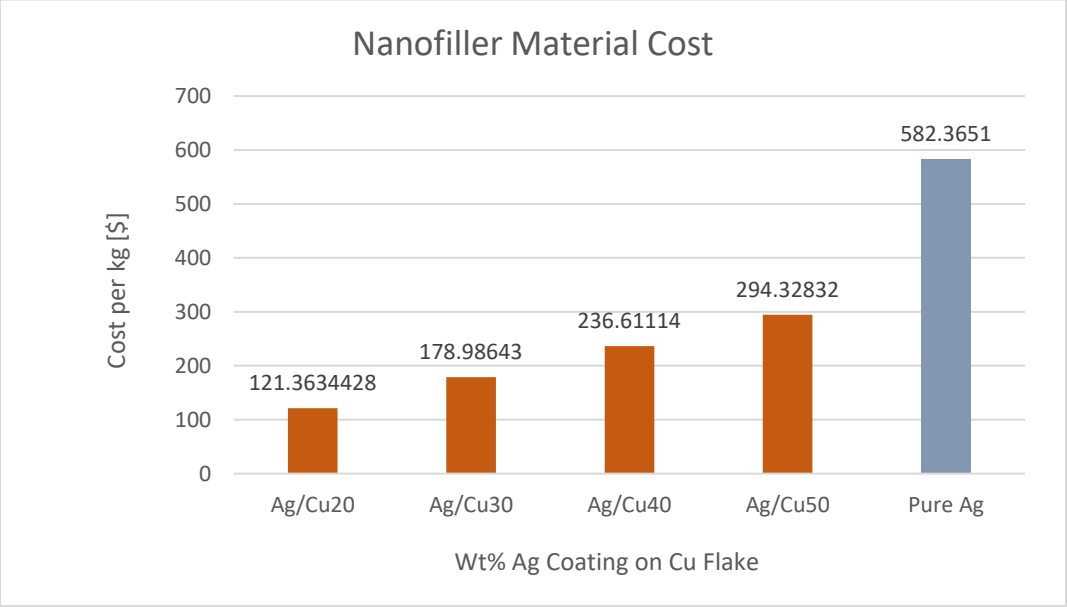

Figure 49. Cost/kg of Ag coated Cu by wt%.

CHAPTER 6

CONCLUSIONS

6.1 Phase One

A spray-coated LSP was developed for use on thermoplastic composites by experimenting with four conductive nano and sub-micro fillers carried by an epoxy resin-based matrix: CNT/GNP, CuNW, and Ag/Cu20 and Ag/Cu30. The two nanofillers that with sufficiently low in resistance after curing in the epoxy matrix were selected to be spray coated on the TPC panels at 55 wt% and 70 wt% loading levels. The CNT/GNP nanofiller was eliminated due to difficulties in producing a sprayable mixture with low enough resistance and high enough loading levels to either disperse current or absorb adequate heat energy before vaporizing. The CuNW nanofiller was found to be less conductive over time, eventually displaying dielectric properties at even 50 wt%. Having been stored in dry form in atmospheric conditions, the assumption was made that the CuNWs had oxidized. Ag/Cu20 was found to be conductive above 35 wt% with sheet resistance as low as 0.7 Ω/sq at 50 wt% and above. Minimum resistance was reached at 70 wt%. Ag/Cu30 was found to be, on average, less than 10% more conductive in trials than Ag/Cu20. The resistance tended to decrease with coating thickness up to about 60 µm. Resistance also increased significantly over time until the coating was oven cured above 85°C for 12 hours.

6.2 Phase Two

Three panels were spray coated with Ag/Cu20 and three with Ag/Cu30. The first panel of each set was coated with an HBN dielectric at 20 wt% loading and then coated with Ag/Cu at 55 wt%. The second panel of each set was only coated with Ag/Cu at 55 wt% loading. The third

panel of each set was coated with 70 wt% Ag/Cu. Difficulties with spray coating the Ag/Cu 70 wt% panels resulted in conductive coatings that were loosely packed and thin compared to the Ag/Cu 55 wt% panels. Despite this, the Ag/Cu panels received no inside damage or delamination. One possible explanation is that the 70 wt% panels with the loosely packed coating projected closer to the paint surface, thereby allowing for greater arc root dispersion and spreading of the energy across the panel surface. One test point on Panel 2 (Ag/Cu20, 55 wt%) resulted in a hole through the panel. The addition of the dielectric neither improved nor reduced the effectiveness of the LSP, making it an unnecessary added weight.

With some development, the Ag/Cu sub-micro flake spray-coated LSP could potentially be an economical alternative to expanded copper foil lightning strike protection for TPC aircraft components that must have post-consolidated LSP.

CHAPTER 7

FUTURE RESEARCH

Improvements could be made to the spray-coating system through improvements to preparation of the mixture and more experimentation with spray gun settings. Low temperature sintering for reducing contact resistance has been explored for conductive nanowire thin films. The feasibility of application within a resin matrix at high loading levels to determine whether an appreciable increase in conductivity is possible is another avenue of exploration.

The fact that only one panel received a hole raises the issue of suitable test parameters such as testing levels, panel thickness, paint thickness, and LSP. Thinner panels are more vulnerable to damage than thicker ones. Future work would include tests with 12-ply laminates.

REFERENCES

REFERENCES

1. Li Y, Li R, Lu L, Huang X. Experimental study of damage characteristics of carbon woven fabric/epoxy laminates subjected to lightning strike. *Compos Part Appl Sci Manuf*. 2015;79:164-175. doi:10.1016/j.compositesa.2015.09.019

2. Gagné M, Therriault D. Lightning strike protection of composites. *Prog Aerosp Sci*. 2014;64:1-16. doi:10.1016/j.paerosci.2013.07.002

3. Li Z, Park JG, Liang Z. High-Performance Multifunctional Thermoplastic Composites Enhanced by Aligned Buckypaper: Multifunctional Thermoplastic Composites. *Adv Eng Mater*. 2016;18(8):1460-1468. doi:10.1002/adem.201600130

4. Kamiyama S, Hirano Y, Okada T, Ogasawara T. Lightning strike damage behavior of carbon fiber reinforced epoxy, bismaleimide, and polyetheretherketone composites. *Compos Sci Technol*. 2018;161:107-114. doi:10.1016/j.compscitech.2018.04.009

5. Chang IY, Lees JK. Recent Development in Thermoplastic Composites: A Review of Matrix Systems and Processing Methods. *J Thermoplast Compos Mater*. 1988;1(3):277-296. doi:10.1177/089270578800100305

6. Larsson A. The interaction between a lightning flash and an aircraft in flight. *Comptes Rendus Phys*. 2002;3(10):1423-1444. doi:10.1016/S1631-0705(02)01410-X

7. ENV-RP-2016-004RevA.pdf. https://www.niar.wichita.edu/agate/Documents/Lightning/ENV-RP-2016-004RevA.pdf. Accessed July 13, 2019.

8. Feraboli P, Miller M. Damage resistance and tolerance of carbon/epoxy composite coupons subjected to simulated lightning strike. *Compos Part Appl Sci Manuf*. 2009;40(6-7):954-967. doi:10.1016/j.compositesa.2009.04.025

9. Hirano Y, Katsumata S, Iwahori Y, Todoroki A. Artificial lightning testing on graphite/epoxy composite laminate. *Compos Part Appl Sci Manuf*. 2010;41(10):1461-1470. doi:10.1016/j.compositesa.2010.06.008

10. Plumer J, Robb J. The Direct Effects of Lightning on Aircraft. *IEEE Trans Electromagn Compat*. 1982;EMC-24(2):158-172. doi:10.1109/TEMC.1982.304010

11. Zhang B, Patlolla VR, Chiao D, Kalla DK, Misak H, Asmatulu R. Galvanic corrosion of Al/Cu meshes with carbon fibers and graphene and ITO-based nanocomposite coatings as alternative approaches for lightning strikes. *Int J Adv Manuf Technol*. 2013;67(5-8):1317-1323. doi:10.1007/s00170-012-4568-3

12. Lightning Protection of Aircraft. *Electro Magn Appl Inc*. https://www.ema3d.com/lightning/lightning-protection-of-aircraft/. Accessed July 13, 2019.

13. Golding W. Lightning Strikes on Commercial Aircraft: How the Airlines Are Coping. *J Aviat Educ Res*. 2005. doi:10.15394/jaaer.2005.1511

14. Uman MA, Rakov VA. The interaction of lightning with airborne vehicles. *Prog Aerosp Sci*. 2003;39(1):61-81. doi:10.1016/S0376-0421(02)00051-9

15. Video Showing What Happens When A Plane Gets Struck By Lightning - MTL Blog. https://www.mtlblog.com/news/video-showing-what-happens-when-a-plane-get-struck-by-lightning. Accessed November 28, 2019.

16. Barbero EJ. *Introduction to Composite Materials Design, Second Edition*. 2 edition. Boca Raton: CRC Press; 2010.

17. Adorni E, Coïsson E, Ferretti D. In situ characterization of archaeological adobe bricks. *Constr Build Mater*. 2013;40:1-9. doi:10.1016/j.conbuildmat.2012.11.004

18. 50 years of reinforced plastic boats. Materials Today. https://www.materialstoday.com/composite-applications/features/50-years-of-reinforced-plastic-boats/. Accessed November 23, 2019.

19. Commercial Aircraft. *Discov Compos*. https://discovercomposites.com/transportation/commercial-aircraft/. Accessed November 23, 2019.

20. Composites Manufacturing: Materials, Product, and Process Engineering. CRC Press. https://www.crcpress.com/Composites-Manufacturing-Materials-Product-and-Process-Engineering/Mazumdar/p/book/9780849305856. Accessed November 18, 2019.

21. Chand S. Review carbon fibers for composites. *J Mater Sci*. 2000;35(6):1303–1313.

22. Engineering Mechanics of Composite Materials. https://www.altobooks.com/app/book.php?isbn=9780195150971&gclid=CjwKCAjwgqbpBRAREiwAF046Jew0R1a61FRrQxcaLmnbI-RNqh657pkLQBtAlyBzXg0dWzU-2jr0EhoCklEQAvD_BwE. Accessed July 13, 2019.

23. Gibson AG, Månson J-A. Impregnation technology for thermoplastic matrix composites. *Compos Manuf*. 1992;3(4):223-233. doi:10.1016/0956-7143(92)90110-G

24. Vaidya UK, Chawla KK. Processing of fibre reinforced thermoplastic composites. *Int Mater Rev*. 2008;53(4):185-218. doi:10.1179/174328008X325223

25. Boeing 787 Update. https://www.compositesworld.com/articles/boeing-787-update. Accessed November 18, 2019.

26. Han J, Zhang H, Chen M, et al. The combination of carbon nanotube buckypaper and insulating adhesive for lightning strike protection of the carbon fiber/epoxy laminates. *Carbon*. 2015;94:101-113. doi:10.1016/j.carbon.2015.06.026

27. Katunin A, Krukiewicz K, Herega A, Catalanotti G. Concept of a Conducting Composite Material for Lightning Strike Protection. *Adv Mater Sci*. 2016;16(2):32-46. doi:10.1515/adms-2016-0007

28. Gou J, Tang Y, Liang F, Zhao Z, Firsich D, Fielding J. Carbon nanofiber paper for lightning strike protection of composite materials. *Compos Part B Eng*. 2010;41(2):192-198. doi:10.1016/j.compositesb.2009.06.009

29. Zhang B. MANUFACTURING, CHARACTERIZATION, AND MODELING OF GRAPHENE-BASED NANOCOMPOSITES FOR AIRCRAFT STRUCTURAL AND LIGHTNING STRIKE APPLICATIONS. :154.

30. Mall S, Ouper BL, Fielding JC. Compression Strength Degradation of Nanocomposites after Lightning Strike. *J Compos Mater*. 2009;43(24):2987-3001. doi:10.1177/0021998309345337

31. Wang B, Duan Y, Xin Z, Yao X, Abliz D, Ziegmann G. Fabrication of an enriched graphene surface protection of carbon fiber/epoxy composites for lightning strike via a percolating-assisted resin film infusion method. *Compos Sci Technol*. 2018;158:51-60. doi:10.1016/j.compscitech.2018.01.047

32. Moisala A, Li Q, Kinloch IA, Windle AH. Thermal and electrical conductivity of single- and multi-walled carbon nanotube-epoxy composites. *Compos Sci Technol*. 2006;66(10):1285-1288. doi:10.1016/j.compscitech.2005.10.016

33. Ma P-C, Siddiqui NA, Marom G, Kim J-K. Dispersion and functionalization of carbon nanotubes for polymer-based nanocomposites: A review. *Compos Part Appl Sci Manuf*. 2010;41(10):1345-1367. doi:10.1016/j.compositesa.2010.07.003

34. Bauhofer W, Kovacs JZ. A review and analysis of electrical percolation in carbon nanotube polymer composites. *Compos Sci Technol*. 2009;69(10):1486-1498. doi:10.1016/j.compscitech.2008.06.018

35. Li QW, Li Y, Zhang XF, et al. Structure-Dependent Electrical Properties of Carbon Nanotube Fibers. *Adv Mater*. 2007;19(20):3358-3363. doi:10.1002/adma.200602966

36. Sreeprasad TS, Berry V. How Do the Electrical Properties of Graphene Change with its Functionalization? *Small*. 2013;9(3):341-350. doi:10.1002/smll.201202196

37. Frank S. Carbon Nanotube Quantum Resistors. *Science*. 1998;280(5370):1744-1746. doi:10.1126/science.280.5370.1744

38. Cortes LQ, Racagel S, Lonjon A, Dantras E, Lacabanne C. Electrically conductive carbon fiber / PEKK / silver nanowires multifunctional composites. *Compos Sci Technol*. 2016;137:159-166. doi:10.1016/j.compscitech.2016.10.029

39. Ha S-W, Mayer J, Koch B, Wintermantel E. Plasma-sprayed hydroxylapatite coating on carbon fibre reinforced thermoplastic composite materials. *J Mater Sci Mater Med*. 1994;5(6-7):481-484. doi:10.1007/BF00058987

40. Mirabella FM, Dioh N, Zimba CG. Theoretical analysis and experimental characterization of the TPO/adhesion promoter/paint interface of painted thermoplastic polyolefins (TPO). *Polym Eng Sci*. 2000;40(9):2000-2006. doi:10.1002/pen.11332

41. Li Y, Zhang H, Liu Y, et al. Synergistic effects of spray-coated hybrid carbon nanoparticles for enhanced electrical and thermal surface conductivity of CFRP laminates. *Compos Part Appl Sci Manuf*. 2018;105:9-18. doi:10.1016/j.compositesa.2017.10.032

42. Bollavaram PK, Rahman MM, Asmatulu R. Lightning Strike Protection and EMI Shielding of Fiber Reinforced Composite Using Gold and Silver Nanofilms. In: *ASME 2018 International Mechanical Engineering Congress and Exposition*. American Society of Mechanical Engineers Digital Collection; 2018.

43. Rathmell AR, Bergin SM, Hua Y-L, Li Z-Y, Wiley BJ. The Growth Mechanism of Copper Nanowires and Their Properties in Flexible, Transparent Conducting Films. *Adv Mater*. 2010;22(32):3558-3563. doi:10.1002/adma.201000775

44. Won Y. Annealing-free fabrication of highly oxidation-resistive copper nanowire composite conductors for photovoltaics | NPG Asia Materials. https://www.nature.com/articles/am201436. Accessed November 26, 2019.

45. Polavarapu L, et al. [45] Preparation of Conductive Silver Films at Mild Temperatures for Printable Organic Electronics | Chemistry of Materials. https://pubs.acs.org/doi/abs/10.1021/cm200471s. Accessed November 28, 2019.

46. 130 Watt Ultrasonic Processors. https://www.thomassci.com/Equipment-and-Instruments/Benchtop-Homogenizers/_/130-WATT-ULTRASONIC-PROCESSORS. Accessed November 28, 2019.

47. Scilogex D500 Homogenizer |@$825.97. https://www.labgearusa.com/scilogex-d500-homogenizer/. Accessed November 28, 2019.

48. Bigand A. Estimation of the load produced by the electro-thermal behaviour of lightning strike protection layers on a composite panel. 2018:9.

49. Foster P, Abdelal G, Murphy A. Quantifying the Influence of Lightning Strike Pressure Loading on Composite Specimen Damage. *Appl Compos Mater*. 2019;26(1):115-137. doi:10.1007/s10443-018-9685-1

APPENDICES

APPENDIX A

TEST PANEL IMAGES

Panel Images: Pre-test

Panel 1: Front

Panel 1: Back

Panel 2: Front

Panel 2: Back

Panel 3: Front

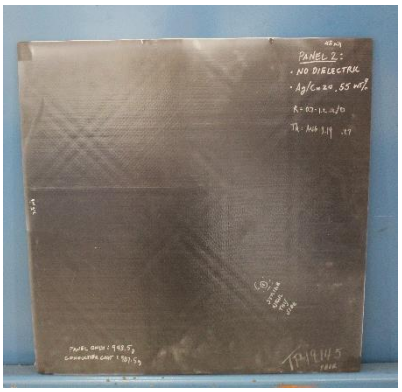

Panel 3: Back

Panel 4: Front

Panel 4: Back

Panel 5: Front

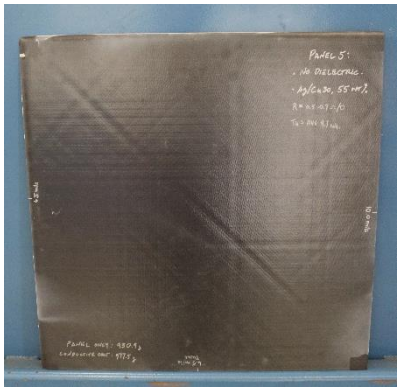

Panel 5: Back

Panel 6: Front

Panel 6: Back

APPENDIX A (continued)

Panel Images: Post-test

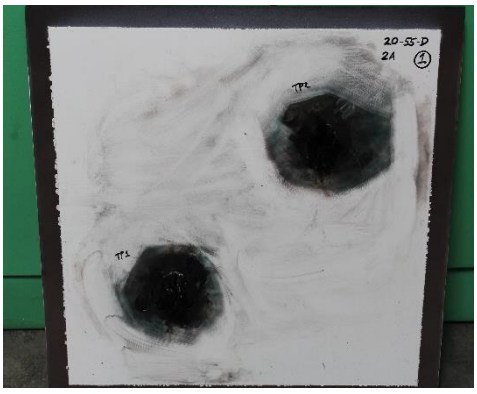

Panel 1: Front

Panel 1: Back

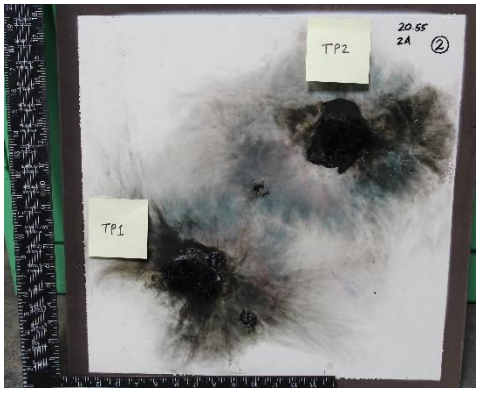

Panel 2: Front

Panel 2: Back

Panel 3: Front

Panel 3: Back

Panel 4: Front

Panel 4: Back

Panel 5: Front

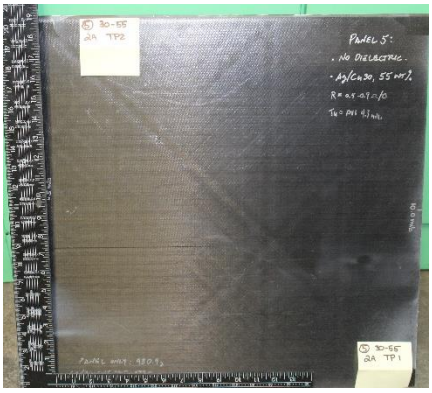

Panel 5: Back

Panel 6: Front

Panel 6: Back

APPENDIX B

SPRAY-COATING EQUIPMENT AND SUPPLIES

Spray-coating Equipment

Manufacturer	Type of Equipment	Equipment Name	Model Number	Serial Number	Used for
BYK	Dry Film Thickness Gauge	PosiTector 6000 Advanced	FNRS3	Body: 748456 Probe: 209801	DFT
Sartorius	SCALE 3KG	Weight Scale	SIWRDCP-1-3-I	26159170	weigh panels + Coatings
Mettler Toledo	SCALE 220G	Weight Scale	XP205	B402180873	weigh matereal in nano fume hood
Qsonica LLC	Sonicator	QSonica	Q700	79012e-02-14	Sonicat batches
Fisher Scientific	Stir / hot plate	Isotemp		C1898140205828	mixing material as it was added to batch
Labconco	Nano fume hood	X Pert Nano		131285618 A	weigh material into beakers
BYK-Gardner	#2 Viscosity cup	S90/ZAHN Signature viscosity cup		71581	viscosity of primer and top coat
VWR	Stopwatch	Traceable Stopwatch		192077324	viscosity of primer and top coat
Fisherbrand	400mL long form glass beaker			FB-102-400	while making Ag/Cu 20, 70wt%, and 30,70wt% Batches
Fisherbrand	400mL KIMAX glass beaker			NO. 14005	while making Ag/Cu 20, 55wt%, and 30,55wt% Batches
Fisherbrand	400mL PYREX glass beaker			NO. 1003	while making Ag/Cu 20, 55wt%, and 30,55wt% Batches

Paint Components

	Material	lot#	Batch#	Part#	MFG	EXP
VWR BDH Chemicals	Isopropyl alcohol	213484				10/16/2022
Sherwin Williams	CM0481968	MQ2762XXXX			10/1/2012	10/1/2013
Sherwin Williams	CM0120828		MZ0458D		2/14/2018	2/14/2020
Sherwin Williams	CM0110933	MQ2788RX			10/5/2018	10/5/2025
Sherwin Williams	Y10942 - white 7568		629560		10/21/2015	10/11/2018
Sherwin Williams	CM0840081	R0440			2/3/2010	2/13/2012
Sherwin Williams	CM0840A03		MZ2220		8/10/2010	8/10/2012
Sherwin Williams	CM0110944	MQ119PP			1/11/2019	1/11/2026

APPENDIX C

GNU OCTAVE CODE FOR CONDUCTIVE COATING CALCULATIONS

```
%Clay Parten
%Nano filler mass/panel calculation
%For 500mm x 500mm panel size (with non-LSP borders excluded)
%INCLUDEs OVERSPRAY of 4" vertical and 4" horizontal per panel
clear all, clc, close all
%aereal_wt = 100; %gsm
disp("THICKNESS of coating [microns]")
thk = 7.9e-5 ;  %thickness in meters
thk_um = thk*1000000
disp("THICKNESS of coating [mils]")
thk_mils = thk*1e6/25.4; %thickness in mils (3 mils compr thk to Dexmet 142gsm or 195gsm)
disp(thk_mils)
disp("(3 mils is equal thickness to Dexmet 142gsm or 195gsm)")
disp("   ")
disp("PANEL LENGTH equals WIDTH [m]")
pnl_h = 0.51 % meters
inches = pnl_h*39.3701
disp("   ")
disp("COATING AREA [m^2]")
area = pnl_h * pnl_h %m^2
disp("COATING AREA [sqft]")
sqft = area*10.7639
disp("   ")
disp("TOTAL COATING VOL per panel [mL]")
vol = thk*area/0.7; %m^3
vol_mL = vol*1e6
disp("   ")
d_3253 = 970; %kg/m^3
d_3282 = 1068; %kg/m^3
d_815C = 1131; %kg/m^3
disp("DENSITY of mixture (resin + curative) [%kg/m^3]")
d_mix = 0.83*d_815C + 0.17*d_3282
disp("   ")
disp("TOTAL MASS per panel with NEAT RESIN/CURATIVE [g]")
m_total = (d_mix*vol)*1000
disp("   ")
vol_tot = 10;
m_resin = 5;
while vol_tot < vol_mL+1
   m_hardener_b = m_resin*0.205;
   RS_b = m_resin + m_hardener_b;
```

```
    nano_50 = (0.50*RS_b)/(1-0.50);
    nano_50_mL = nano_50/5;
    vol_tot = (RS_b/(d_mix/1000))+nano_50_mL;
    m_resin = m_resin+1;
end
ending_vol = vol_tot
N_50_vol = nano_50_mL
Vol_815C_and_3282 = vol_tot - nano_50_mL
N_50_mass = N_50_vol*5
Mass_815C_and_3282 = Vol_815C_and_3282*d_mix/1000
m_resin = m_resin -1
m_hardener_b = m_resin*0.205
Total_mass = Mass_815C_and_3282 + N_50_mass
disp("   ")
vol_tot = 10;
m_resin = 5;
while vol_tot < vol_mL+1
    m_hardener_b = m_resin*0.205;
    RS_b = m_resin + m_hardener_b;
    nano_55 = (0.55*RS_b)/(1-0.55);
    nano_55_mL = nano_55/5;
    vol_tot = (RS_b/(d_mix/1000))+nano_55_mL;
    m_resin = m_resin+1;
end
ending_vol = vol_tot
N_55_vol = nano_55_mL
Vol_815C_and_3282 = vol_tot - nano_55_mL
N_55_mass = N_55_vol*5
Mass_815C_and_3282 = Vol_815C_and_3282*d_mix/1000
m_resin = m_resin -1
m_hardener_b = m_resin*0.205
Total_mass = Mass_815C_and_3282 + N_55_mass
disp("   ")
vol_tot = 10;
m_resin = 5;
while vol_tot < vol_mL+1
    m_hardener_b = m_resin*0.205;
    RS_b = m_resin + m_hardener_b;
    nano_70 = (0.70*RS_b)/(1-0.70);
    nano_70_mL = nano_70/5;
    vol_tot = (RS_b/(d_mix/1000))+nano_70_mL;
    m_resin = m_resin+1;
end
```

```
ending_vol = vol_tot
N_70_vol = nano_70_mL
Vol_815C_and_3282 = vol_tot - nano_70_mL
N_70_mass = N_70_vol*5
Mass_815C_and_3282 = Vol_815C_and_3282*d_mix/1000
m_resin = m_resin -1
m_hardener_b = m_resin*0.205
Total_mass = Mass_815C_and_3282 + N_70_mass
disp("   ")
disp("Volume for 2 panels including Solvent [mL]")
VOL_Two = ending_vol*1.8*2
disp("   ")
disp("Volume for 3 panels including Solvent [mL]")
VOL_Three = ending_vol*1.8*3
```